Atmos. Chem. Phys., 14, 3657–3690, 2014
www.atmos-chem-phys.net/14/3657/2014/
doi:10.5194/acp-14-3657-2014

Atmospheric Chemistry and Physics Open Access

Multi-decadal aerosol variations from 1980 to 2009: a perspective from observations and a global model

Mian Chin[1], T. Diehl[1,2,*], Q. Tan[1,2], J. M. Prospero[3], R. A. Kahn[1], L. A. Remer[4], H. Yu[1,5], A. M. Sayer[1,2], H. Bian[1,4], I. V. Geogdzhayev[6,7], B. N. Holben[1], S. G. Howell[8], B. J. Huebert[8], N. C. Hsu[1], D. Kim[1,2], T. L. Kucsera[1,2], R. C. Levy[1], M. I. Mishchenko[6], X. Pan[1], P. K. Quinn[9], G. L. Schuster[10], D. G. Streets[11], S. A. Strode[1,2], O. Torres[1], and X.-P. Zhao[12]

[1]NASA Goddard Space Flight Center, Greenbelt, MD, USA
[2]Universities Space Research Association, Columbia, MD, USA
[3]University of Miami, Miami, FL, USA
[4]University of Maryland, Baltimore County, Baltimore, MD, USA
[5]University of Maryland, College Park, College Park, MD, USA
[6]NASA Goddard Institute for Space Studies, New York, NY, USA
[7]Columbia University, New York, NY, USA
[8]University of Hawaii, Honolulu, HI, USA
[9]NOAA Pacific Marine Environmental Laboratory, Seattle, WA, USA
[10]NASA Langley Research Center, Hampton, VA, USA
[11]Argonne National Laboratory, Argonne, IL, USA
[12]NOAA National Climatic Data Center, Asheville, NC, USA
[*]currently at: Joint Research Center, European Commission, Ispra, Italy

Correspondence to: Mian Chin (mian.chin@nasa.gov)

Received: 9 July 2013 – Published in Atmos. Chem. Phys. Discuss.: 26 July 2013
Revised: 30 January 2014 – Accepted: 21 February 2014 – Published: 10 April 2014

Abstract. Aerosol variations and trends over different land and ocean regions from 1980 to 2009 are analyzed with the Goddard Chemistry Aerosol Radiation and Transport (GOCART) model and observations from multiple satellite sensors and available ground-based networks. Excluding time periods with large volcanic influence, aerosol optical depth (AOD) and surface concentration over polluted land regions generally vary with anthropogenic emissions, but the magnitude of this association can be dampened by the presence of natural aerosols, especially dust. Over the 30-year period in this study, the largest reduction in aerosol levels occurs over Europe, where AOD has decreased by 40–60 % on average and surface sulfate concentrations have declined by a factor of up to 3–4. In contrast, East Asia and South Asia show AOD increases, but the relatively high level of dust aerosols in Asia reduces the correlation between AOD and pollutant emission trends. Over major dust source regions, model analysis indicates that the change of dust emissions over the Sahara and Sahel has been predominantly driven by the change of near-surface wind speed, but over Central Asia it has been largely influenced by the change of the surface wetness. The decreasing dust trend in the North African dust outflow region of the tropical North Atlantic and the receptor sites of Barbados and Miami is closely associated with an increase of the sea surface temperature in the North Atlantic. This temperature increase may drive the decrease of the wind velocity over North Africa, which reduces the dust emission, and the increase of precipitation over the tropical North Atlantic, which enhances dust removal during transport. Despite significant trends over some major continental source regions, the model-calculated global annual average AOD shows little change over land and ocean in the past three decades, because opposite trends in different land regions cancel each other out in the global average, and changes over large open oceans are negligible. This highlights the necessity for regional-scale

assessment of aerosols and their climate impacts, as global-scale average values can obscure important regional changes.

1 Introduction

Aerosols affect earth's energy budget by scattering and absorbing solar and terrestrial radiation and by altering cloud properties and lifetimes. They also influence weather, air quality, atmospheric chemistry, and biogeochemical cycles. Anthropogenic activities have caused considerable changes in aerosol composition and loading, and will continue to do so in the future (e.g., Leibensperger et al., 2012; Sillmann et al., 2013). Historical emission inventories have estimated that trends in anthropogenic emission are closely tied to economic growth, population density, and technological development, which may explain the regional aerosol variability shown in the long-term satellite data records. Furthermore, long-term trends in observed surface solar radiation generally mirror aerosol emission trends (e.g., Streets et al., 2006), implying a link between aerosol forcing and solar "dimming" and "brightening". Understanding the cause of aerosol trends in terms of human activities or natural variability is key to projecting the earth system's response to future changes.

Satellite observations of global aerosol distributions started over three decades ago with the Total Ozone Mapping Spectrometer (TOMS) and Advanced Very High Resolution Radiometer (AVHRR). Although these instruments were not specifically designed to measure aerosols, thus having limited accuracy and retrievable information, they provide a long-term perspective on changes over different regions of the world. More recent satellite sensors, such as the Sea-viewing Wide Field-of-view Sensor (SeaWiFS), the Moderate Resolution Imaging and Spectroradiometer (MODIS), and the Multiangle Imaging Spectroradiometer (MISR) instruments included on the Earth Observing System (EOS) satellites have an improved accuracy and enhanced capability to retrieve aerosol amount, distribution, and physical/optical properties. Although the EOS data records are not long enough to derive multi-decadal trends, they can be compared with AVHRR and TOMS for the overlapping time periods in order to assess their consistency. At this time, however, it is still difficult to unambiguously determine the origin and composition of aerosols using satellite data alone.

Complementing global satellite observations are several ground-based networks monitoring the changes of aerosols in the past decades. They include aerosol optical depth (AOD) measurements from the world-wide Aerosol Robotic Network (AERONET, Holben et al., 1998, 2001) and surface concentration measurements of aerosol species from several coordinated networks, such as the Interagency Monitoring of Protected Visual Environments (IMPROVE, Malm et al., 1994, 2003) over the United States, the European Monitoring and Evaluation Programme (EMEP) network over Europe (http://www.emep.int/), the University of Miami's measurement program at sites over several oceanic islands (e.g., Prospero, 1999; Prospero et al., 2003; Prospero and Lamb, 2003; Savoie et al., 2002), and measurements over several Arctic sites (Quinn et al., 2007, 2008) that were used in the Arctic Monitoring and Assessment Program. Although spatial and/or temporal coverage of these data are limited, they provide more detailed information on aerosol properties, long-term variations, and/or measurement accuracy for satellite and model validation.

Numerous studies have assessed aerosol trends over various spatial domains and time periods. For example, Luo et al. (2001) estimated AOD changes based on the solar radiation data over 46 stations in China and found a significant AOD increase from 1976 to 1990. Massie et al. (2004) used the wintertime TOMS AOD over Asia as a proxy for anthropogenic AOD and found a 17 % increase per decade between 1979 and 2000 over the coastal plains in China and the Ganges River basin in India. The analyses of MISR (Dey and Di Girolamo, 2011), MODIS (Ramachandran et al., 2012) and surface network data (Moorthy et al., 2012) over India showed a statistically significant increase in AOD over many locations between 2000 and 2009, attributed mostly to the increase in anthropogenic aerosols. In contrast, global model simulations (Leibensperger et al., 2012) and IMPROVE measurements over the US (Murphy et al., 2011; Collaud Coen et al., 2013) indicated a decreasing trend in aerosol concentrations, extinction, and wet deposition fluxes from 1990 to the 2000s. A similar decrease in AOD was also found over Europe from the late 1980s to the late 2000s based on model simulations and measurements (Chiacchio et al., 2011). Meanwhile, a decrease in sulfate concentration measured at a site in Israel from the 1980s into the 2000s was linked to the decreasing sulfur emissions in eastern Europe (Karnieli et al., 2009). Global analysis of satellite data from SeaWiFS between 1997 and 2010 (Hsu et al., 2012) showed a large upward trend in AOD over the Arabian Peninsula as well as an increase over China and India, but a decrease over the US and Europe. Surface sulfate aerosol concentrations over the Arctic have also declined, with the magnitude of the decline dependent on location and time period (Quinn et al., 2007). The changes over ocean, however, are less clear, and different satellite products seem to disagree on the direction of changes in the past decade (Mishchenko et al., 2007, 2012; Remer et al., 2008; Yu et al., 2009; Thomas et al., 2010; Zhang and Reid, 2010; Hsu et al., 2012; Zhao et al., 2008, 2013). However, "bias-corrected" MODIS and MISR data, which underwent additional processing to remove cloud contamination and correct wind or microphysical effects on AOD retrieval, showed a statistically negligible global-average trend over ocean from 2000 to 2009, as well as regional trends similar to those obtained from ground-based measurements (Zhang and Reid, 2010).

Expanding from the trend studies mentioned previously, the present study provides a unique, comprehensive synthesis and assessment of aerosol variations over the last three decades (1980–2009) in different regions of the globe using a global model analysis and multiple-platform data sets, with the goal of determining the anthropogenic and natural contributions to the multi-decadal changes. We also use the model to examine the relationships between emission, surface concentration, and column AOD, and the factors controlling the long-term variations of dust aerosols. We use the Goddard Chemistry Aerosol Radiation and Transport (GOCART) model, which incorporates aerosol and precursor emissions from fossil fuel/biofuel combustion, biomass burning, and natural sources (volcanoes, deserts, and oceans), and is driven by the meteorological-reanalysis fields, to simulate aerosol distributions from 1980 to 2009. We consider fifteen land and twelve ocean regions in our analysis (regional domains shown in Fig. 1; region names and surface areas listed in Table 1). The land regions are generally defined according to the geopolitical boundaries of countries or regions to better connect the aerosol changes with regional economic development and environmental policies.

In the rest of this paper, we first describe the GOCART model simulations in Sect. 2 and the long-term observations used in this study in Sect. 3. We show the results of model-to-data comparisons in Sect. 4, addressing global distributions (Sect. 4.1), regional trends in AOD and surface concentrations over selected land (Sect. 4.2) and ocean (Sect. 4.3) areas, and global change patterns (Sect. 4.4), followed by a synopsis of the results (Sect. 4.5). We then discuss in Sect. 5 the relationship between anthropogenic emission and atmospheric burden (Sect. 5.1), the controlling factors of dust change (Sect. 5.2), and the significance of global trends (Sect. 5.3). Conclusions are given in Sect. 6.

This is the first part of our analysis of long-term aerosol variations and its environmental effects. It also serves as an introduction and background for other manuscripts currently under preparation that address aerosol effects on surface radiation and source–receptor relationships.

Table 1. Region description, abbreviation, and surface area of 15 land and 12 ocean regions (domains in Fig. 1).

	Region	Abbr.	Area (10^9 m^2)
Land regions			
L-01	Canada + Alaska	CAN	13 350
L-02	United States (Continental)	USA	8200
L-03	Central America + Mexico	CAM	3900
L-04	South America	SAM	18 980
L-05	Europe	EUR	7480
L-06	Russia + Georgia	RUS	18 230
L-07	Central Asia	CAS	3930
L-08	Middle East	MDE	6650
L-09	East Asia	EAS	12 190
L-10	South Asia	SAS	5460
L-11	Southeast Asia	SEA	7640
L-12	Australia and New Zealand	ANZ	9260
L-13	Sahara	SHR	9230
L-14	Sahel	SHL	2980
L-15	Rest of Africa	RAF	19 300
Ocean regions			
O-01	North Atlantic	NAT	20 960
O-02	Central Atlantic	CAT	22 490
O-03	South Atlantic	SAT	30 370
O-04	Western North Pacific	WNP	10 600
O-05	Western Central Pacific	WCP	23 170
O-06	Western South Pacific	WSP	17 420
O-07	Eastern North Pacific	ENP	14 030
O-08	Eastern Central Pacific	ECP	29 820
O-09	Eastern South Pacific	ESP	54 520
O-10	North Indian Ocean	NIN	9750
O-11	South Indian Ocean	SIN	42 870
O-12	Southern Ocean	SOU	53 580

2 Simulations of aerosols with the GOCART model

2.1 GOCART model

The GOCART model has been described in detail in our previous publications (e.g., Chin et al., 2000, 2002, 2007, 2009; Ginoux et al., 2001, 2004) and also in the Supplement (Sect. S1) for the current version. Here, we provide a brief summary to describe recent key updates and also to facilitate the discussion. For the present work, the meteorological fields from the Modern-Era Retrospective Analysis for Research and Applications (MERRA) (Rienecker et al., 2011), produced with version 5 of the Goddard Earth Observing System Data Assimilation System (GEOS5-DAS), are used with a GOCART configuration at a horizontal resolution of 2.5° longitude by 2° latitude and 72 vertical levels from the surface to 0.01 hPa. Aerosol simulations in GOCART include the major aerosol types of sulfate, dust, black carbon (BC), organic matter (OM) (or organic carbon OC, typically $\mathrm{OM} = \mathrm{OC} \cdot f$ with $f = 1.4$–2.2 in the literature), and sea salt, and the precursor gas species of SO_2 and dimethyl sulfide (DMS). It also contains another natural aerosols species, methanesulfonate (MSA, also known as methanesulfonic acid), which is formed from a branch of DMS oxidation. The model accounts for emissions from fossil fuel and biofuel combustion, biomass burning, volcanic eruptions, vegetation, deserts, and oceans. A recent update includes improvements of dust emissions that consider the seasonal and interannual variability of vegetation coverage (Kim et al., 2013; see Sect. 2.2) and dust optical properties that are calculated with the T-matrix code (Dubovik et al., 2006) to account for the non-spherical shape of dust particles (Mishchenko et al., 1997).

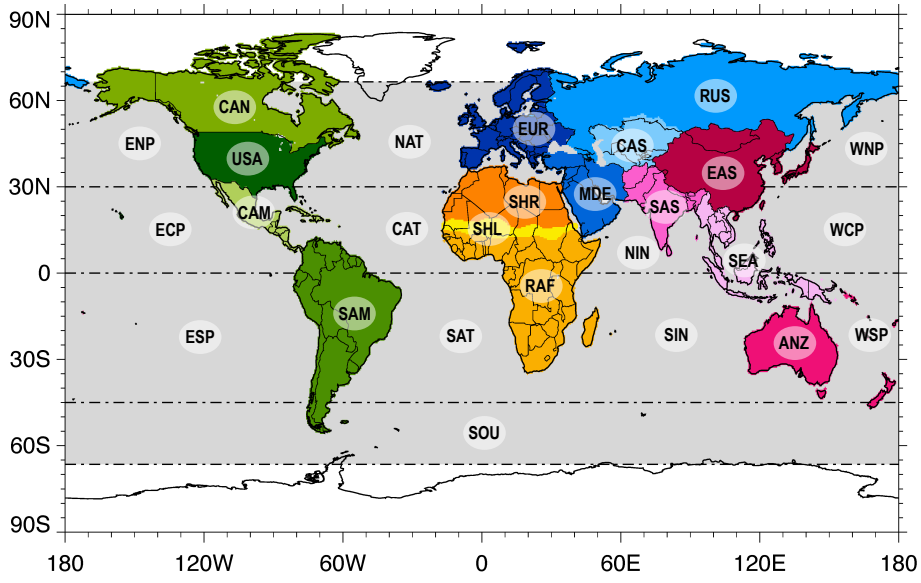

Fig. 1. Land and ocean region domains defined in this study. Region description, abbreviation, and surface area listed in Table 1. Regions with names in the circles are discussed in the text.

2.2 Emissions from 1980 to 2009

Table 2 summarizes the emission data sets used or methods of calculating emissions in the GOCART model, and more detailed information is given in the Supplement. Briefly, emissions of SO_2, BC, and OC from fossil fuel and biofuel combustion and biomass burning are taken from the emission data set A2-ACCMIP (Diehl et al., 2012), which is one of the multi-year emission data sets available from the international initiative AeroCom project for its second phase (A2) hindcast model experiments (http://aerocom.met.no). We choose to use this emission data set because of its broad acceptance in modeling communities and extended time coverage. The annually variable A2-ACCMIP biomass burning emissions from 1980 to 2009 are presented in Granier et al. (2011) and Diehl et al. (2012), and are typically lower than the emission from our previous studies (e.g., Chin et al., 2009) by 30–50 % for BC and 0–50 % for OC, depending on vegetation type (Petrenko et al., 2012). Volcanic SO_2 emissions are taken from a recently compiled database (A2-MAP) that incorporates information from the Smithsonian Institution's Global Volcanism Program (http://www.volcano.si.edu/), the satellite observations of SO_2 from the Total Ozone Mapping Spectrometer (TOMS) and the Ozone Monitoring Instrument (OMI), and ancillary information from other observations reported in the literature. It also includes emissions from quasi-continuously erupting and silently degassing volcanoes (see Diehl et al., 2012 and references therein). Dust emissions are calculated as a function of surface topography, surface bareness, 10 m wind speed $u_{10\,\mathrm{m}}$, and ground wetness w (Ginoux et al., 2001). Here w is the fraction of surface area in each model grid cell that is wet (dimensionless, varying between 0 and 1), which is used to calculate the threshold wind velocity for dust emission as well as to serve as a switch such that dust will only be mobilized when w is below a threshold value. A recent update of surface bareness, based on the 8 km Normalized Difference Vegetation Index (NDVI) data from AVHRR at twice-per-month time resolution (Tucker et al., 2005; Brown et al., 2006), allows seasonal and interannual variation of the surface bareness in semi-arid areas to regulate the dust emission (details in Kim et al., 2013).

Figure 2 shows the emissions from fossil fuel/biofuel combustion, biomass burning, and major natural sources from 1980 to 2009 used in this study (spatial patterns of emissions from different sources are displayed in the Supplement, Fig. S1). In addition to global total emissions (black circles on top of grey-shaded area in Fig. 2), emissions from several important source regions are also plotted (colored lines). There are large differences among regions in amount emitted and trends. For example, fossil fuel and biofuel sources of SO_2 in USA and Europe (EUR) have decreased by 60 % and 80 %, respectively, from 1980 to 2009, whereas that in East Asia (EAS) and South Asia (SAS) show the opposite trend as the emissions have increased by a factor of 2 in EAS and by more than a factor of 4 in SAS. Emissions of BC and OC from fuel combustion sources display similar regional tendencies, although the magnitude of change is smaller than the SO_2 emissions. Biomass burning emissions, on the other hand, demonstrate considerable interannual and regional variability. The strongest volcanic emission within the 30-year period is from the eruption of Mt. Pinatubo (located in the Philippines) in 1991, which injected about 20 Tg (10^{12} g) SO_2 into the stratosphere (e.g., Bluth et al., 1992; McCormick et al., 1995). Other significant volcanic

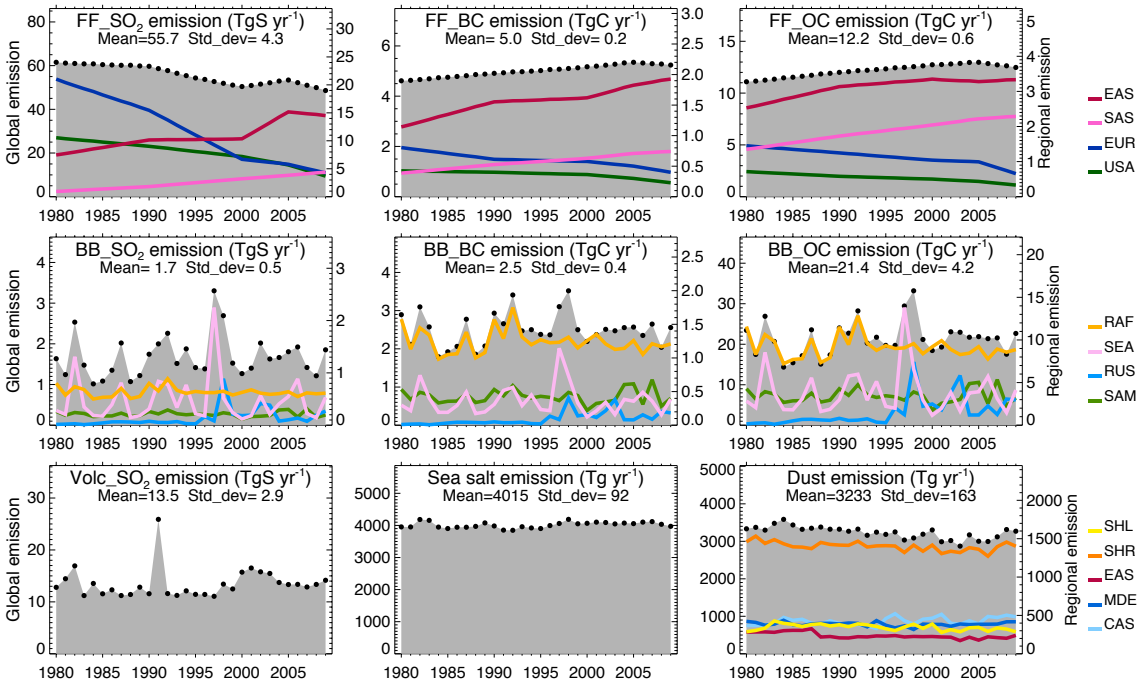

Fig. 2. Emissions from fossil fuel/biofuel (FF) (top row) and biomass burning (BB) (middle row) sources shown as global total (black circles on top of the grey shaded area, left *y* axis scale) and from major source regions (colored lines, right *y* axis scale) of SO_2 (left), BC (middle), and OC (right). Bottom row showing total volcanic SO_2 (left), sea salt (middle), and total and regional dust emissions (right, regional emission in colored lines with scale on right *y* axis). Region domains in Fig. 1 and names in Table 1. The 30-year mean values and standard deviation of the total annual emission are listed on each panel.

eruptions during this period include El Chichón (in Mexico) in 1982 and Miyakajima (in Japan) that erupted in summer 2000 and continued for a few years. Sea salt and dust emissions also vary year to year, driven mainly by the 10 m wind speeds but also affected by other surface parameters.

2.3 Model simulations

Using the model configurations and emissions described in Sects. 2.1 and 2.2, we conducted two 30-year GOCART simulations from 1980 to 2009 (with 6-month spin up): a "standard" simulation that includes all emissions of aerosols and precursor gases, and a "natural" simulation that considers only emissions from natural sources, i.e., deserts, oceans, vegetation, and volcanoes. The differences between the standard and natural runs are attributed to the contributions from fossil fuel/biofuel combustion and biomass burning sources. We refer to these sources collectively as "combustion" sources, or "FF+BB", which are mostly of anthropogenic origin (although a fraction of biomass burning is natural, i.e., triggered by lightning, especially in boreal regions). These model experiments are used to assess the composition and origin of aerosols and their change over the 30-year period covered by this study.

3 Long-term observations of aerosols

Aerosol data products from remote sensing and in situ measurements, together with associated time periods and measured quantities used in this study are listed in Table 3, including AOD from six satellite retrievals, AOD from ground-based AERONET measurements, and surface concentration from the IMPROVE, EMEP, and University of Miami networks and the Arctic. All data used in this study are monthly averages, with the AOD data at 550 nm (TOMS at 500 nm). The satellite data are the gridded (i.e., "level 3") products at $1^\circ \times 1^\circ$ resolution. Brief descriptions of each data set are given below. Additional information on data quality is given in the Supplement (Sect. S2).

3.1 AOD from satellite retrievals

Satellite remote sensing of aerosols started more than three decades ago with the TOMS (Hsu et al., 1996; Herman et al., 1997; Torres et al., 1998, 2002) and AVHRR instruments (Stowe et al., 1997; Husar et al., 1997). Despite limitations in accuracy and retrievable information, these observations provide a long-term perspective on regional aerosol changes over global scales. Several retrieval algorithms have been used to extract AOD from the AVHRR-measured radiation reflected by the atmosphere–surface system (e.g., Stowe et

Table 2. Emissions used in the present study*.

Emission source	Emitted species	Emission data sets/Methods	Reference
Fossil fuel/biofuel combustion, land-based	SO_2, BC, OC, sulfate	A2-ACCMIP (ACCMIP 1980–2000, RCP8.5 2000–2009, linearly interpolated from the decadal/ half decadal increments)	Lamarque et al. (2010); Riahi et al. (2011); Granier et al. (2011); Diehl et al. (2012)
Fuel combustion, international shipping	SO_2, BC, OC	A2-MAP (EDGAR 32FT2000, interpolated)	Diehl et al. (2012) and references therein
Fuel combustion, aircraft	SO_2, BC, OC	A2-MAP (constructed and interpolated from several data sets)	Diehl et al. (2012) and references therein
Biomass burning	SO_2, BC, OC	A2-ACCMIP (RETRO 1980–1997, GFED v2 1997–2008, RCP8.5 2009)	Granier et al. (2011); Diehl et al. (2012), and references therein
Volcanic	SO_2	A2-MAP data set (1167 active volcanoes from 1979 to 2009 based on the Global Volcanism Program, TOMS and OMI satellite retrieved SO_2, and including degassing volcanoes)	Diehl et al. (2012) and references therein
Terrestrial biogenic	OC	Monthly monoterpene emissions from vegetation converted to secondary OC	Guenther et al. (1995); Chin et al. (2002)
Ocean biogenic	DMS	Calculated as a function of sea surface water DMS concentrations, sea water viscosity, and 10 m winds	Lana et al. (2011); Chin et al. (2002)
Deserts	Dust	Calculated as a function of surface bareness, surface topographic features, 10 m wind speed ($u_{10\,m}$), and ground wetness (w)	Ginoux et al. (2001); Kim et al. (2013)
Ocean	Sea salt	Calculated as a function of 10 m wind speed	Gong et al. (2003); Chin et al. (2002); Chin et al. (2009)

*More detailed descriptions of the emission data sets in the Supplement.

Table 3. Observation data used in the present study.

Data set	Location	Period
Satellite AOD		
AVHRR[a]-CDR	Global, ocean	1981–2009
AVHRR[a]-GACP	Global, ocean	1981–2005
TOMS[b]	Global, land +ocean	1980–1992, 1996–2001
SeaWiFS	Global, land +ocean	1997–2009
MISR	Global, land +ocean	2000–2009
MODIS-Terra	Global, land +ocean	2000–2009
MODIS-Aqua	Global, land +ocean	2002–2009
Sun photometer AOD sites with $\geq$ 12 years of measurements		
AERONET	15 sites over land and islands	1995–2009
Surface aerosol species concentration at sites with $\geq$ 15 years of measurements		
IMPROVE	44 sites in US	1988–2007
EMEP	64 sites in Europe	1980–2008
Arctic	2 sites in the Arctic	1980–2009
Univ. Miami	4 sites on islands or coast	1980–2009
Univ. Hawaii	1 site, Mauna Loa, Hawaii	1989–2009

[a]AVHRR instrument onboard 12 different NOAA satellites (NOAA-6, -7, -9, -10, -11, -12, -14, -15, -16, -17, -18, and -19) during the study period.
[b]TOMS instrument onboard the Nimbus-7 satellite between 1979 and 1992 and the Earth Probe satellite between later half of 1996 and 2005. Data quality degraded after 2001, thus not used here. No TOMS data available between 1993 and first half of 1996.

al., 1997; Nakajima and Higurashi 1998; Mishchenko et al. 1999, 2007, 2012; Zhao et al., 2008, 2013). In this study, we use two AVHRR AOD data sets, one produced by the NOAA Climate Data Record (CDR) project (Chan et al., 2013; Zhao et al., 2013; referred to as AVHRR-CDR hereafter) and the other from the Global Aerosol Climatology Project (GACP, Mishchenko et al., 2012, referred to as AVHRR-GACP hereafter), for their improved accuracy over the earlier operational products due to calibration adjustments and retrieval algorithms upgrades. Because of the relatively bright and highly variable land surface reflectance at the visible wavelengths, the AVHRR retrievals have so far been mostly restricted to oceans (e.g., Stowe et al., 1997). On the other hand, the TOMS aerosol product covers both land and ocean from its UV wavelength detection capability, for which the surface signal reaching the top of the atmosphere is usually small. However, because of the coarse instrument spatial resolution ($\sim$ 50 km pixel size at nadir), removing cloud contamination for aerosol retrievals is difficult, which has hampered both the aerosol retrieval availability and data quality (see next section), so the uncertainties associated with the TOMS AOD products are relatively large (Torres et al., 2002, 2005).

More recent satellite sensors on board a series of NASA's Earth Observing System (EOS) satellites, launched in the late 1990s or early 2000s, have much improved accuracy and enhanced capability for retrieving aerosol amount, distribution, and physical/optical properties, allowing more reliable assessments of aerosol changes, albeit over a relatively short observation period. They include the SeaWiFS (McLain et al., 1998; Hsu et al., 2004, 2012; Sayer et al., 2012), MISR on the EOS-Terra satellite (Kahn et al., 2009, 2010), and MODIS on both EOS-Terra and EOS-Aqua satellites (Kaufman et al., 1997; Tanré et al., 1997; Remer et al., 2005, 2008; Levy et al., 2010, 2013), with aerosol products covering both land and ocean. The MODIS AOD product used here is from a combination of the "dark target" retrieval (collection 5.1) that provides global AOD coverage except over bright desert surfaces (Levy et al., 2010) and the "deep blue" retrieval, which uses the 412 nm channel of MODIS to enable the retrieval of AOD over bright surfaces over land (Hsu et al., 2004).

For trend analysis, the monthly average, gridded satellite products are further averaged to yield annual mean values. Note that because of the differences in instrument capabilities and swath widths, the spatial and temporal coverage of the data for calculating monthly average can be quite different among the satellite products. For example, MISR's relatively narrow swath (380 km) limits its global coverage to every 9 days at the equator and every 4–5 days at 60° latitude (although its multi-angle capability does capture over-ocean areas that are in sun glint for single-view instruments), whereas MODIS, with its 6 times-wider swath (2330 km), provides near daily coverage (although still gaps at the equator and sun glint areas over ocean); TOMS has more missing data in partially cloudy scenes than higher resolution instruments due to its larger pixel size. In addition, at high latitudes, the annual mean values of satellite products are biased toward summer months because of the lengthy darkness in the winter months prohibiting AOD retrieval at UV and visible wavelengths.

3.2 AOD from AERONET measurements

The AERONET program is a worldwide ground-based sun photometer network (Holben et al., 1998, 2001; Eck et al., 1999) that started in the mid-1990s with about a dozen sites and has since grown to include over a few hundred sites (http://aeronet.gsfc.nasa.gov). Because of the direct measurements and unified high standard for instrument calibration, AERONET AOD data are considered as "ground truth" and are widely used for satellite products validation and model evaluations. However, most AERONET sites started AOD measurements in the 2000s and some sites have only short periods of data coverage (e.g., as a part of field experiments); only 15 sites provide relatively long and continuous records from the 1990s to 2009 (Fig. 3, left panel) that are more appropriate for information on changes beyond the decadal timescale. Here we use data from six such sites (shown in squares in Fig. 3, left panel) in pollution, dust, and biomass burning source regions to provide complementary information of aerosol trends and to evaluate the model and satellite products.

3.3 Surface concentration measurements

Over the past two to three decades, several surface measurement networks were established to continuously monitor aerosol and precursor concentrations. However, these are mostly located in North America and Europe; there are essentially no long-term aerosol concentration measurement networks or monitoring sites in developing countries. In this study we use the surface measurements from: (1) the Interagency Monitoring of Protected Visual Environments (IMPROVE, Malm et al., 1994, 2003) network over the US, which routinely measures aerosol chemical composition and aerosol extinction at the surface, mostly in national park areas since 1988; (2) the co-operative program for monitoring and evaluating the long-range transmissions of air pollutants in Europe (EMEP) network, which has collected aerosol data in Europe since the late 1970s with most long-term data limited to the "acidifying" (e.g., sulfur) species; (3) the University of Miami-operated network over several islands in the Pacific, Atlantic, and Southern Ocean locations, mostly from the 1980s to 1990s and a few lasting into the 2000s (e.g., Prospero et al., 1999; Maring et al., 2000; Savoie et al., 2002), plus a University of Hawaii site at Mauna Loa Observatory with sulfate and MSA data since 1989, and (4) Arctic stations (Quinn et al., 2007, 2008; Arctic Monitoring and Assessment Program, http://www.amap.no) with long-term data

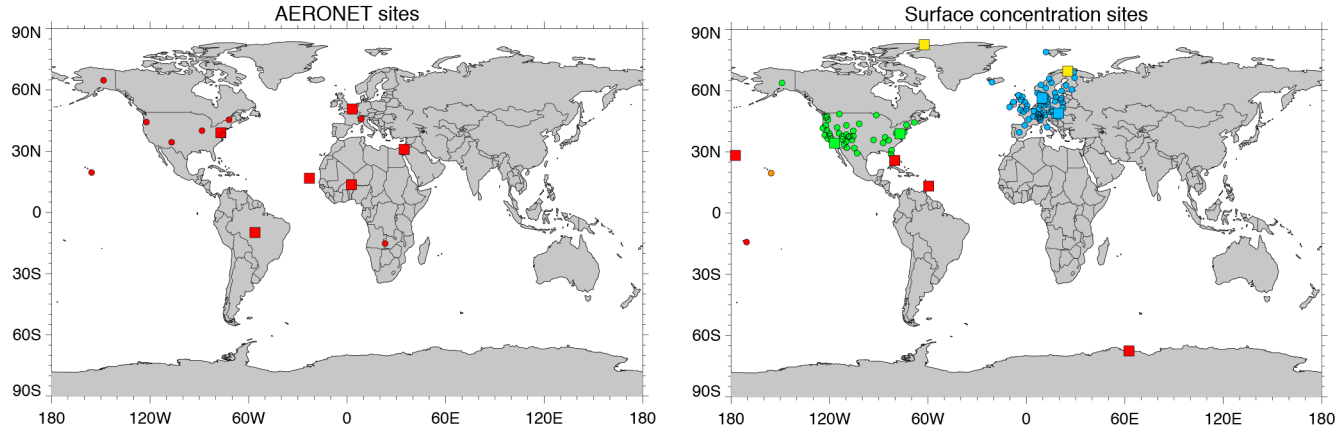

Fig. 3. (left) Locations of 15 AERONET sun photometer sites with at least 12-year AOD data record, and (right) locations of 44 IMPROVE network sites in the US (green), 64 EMEP network sites in Europe (blue), 5 University of Miami sites in the ocean islands (red), University of Hawaii site at Mauna Loa (orange), and 2 Arctic sites (yellow) with at least 15-year data records for at least one aerosol quantity (e.g., sulfate) except the Mawson Station on the Antarctic coast, which had only 9 years of measurements. Mawson is included for its unique remote location. The sites where data are shown in Figs. 7, 8, and 10 are indicated with larger square symbols. (The shorter time span criteria for AERONET is because of its relatively shorter history such that only 3 sites have 15 years of data from 1995 to 2009.)

mostly limited to inorganic species such as sulfate, nitrate, and ammonia (Quinn et al., 2007 and references therein). All data are monthly averages. Locations of the surface sites are plotted in Fig. 3 (right panel, with selected sites discussed in Sect. 4 shown in squares).

4 Results

In this section, we assess the aerosol multi-decadal trends and variations in different regions. We show the spatial patterns of global aerosol spatial distributions from multiple satellite data sets and the GOCART model (Sect. 4.1), multi-decadal variations of regional AOD and aerosol surface mass concentrations over land (Sect. 4.2) and ocean (Sect. 4.3), and spatial patterns of AOD change over two time segments during the past 30 years (Sect. 4.4). Because of a large amount of material covered in this section, a synopsis is given at the end (Sect. 4.5).

4.1 Global AOD distributions

Global distributions of annual averaged AOD at 550 nm for 2001 from AVHRR-CDR, AVHRR-GACP, TOMS, SeaWiFS, MODIS-Terra, and MISR are displayed in Fig. 4 (row 1–2). The year 2001 was chosen because of all the above satellite data available in that year (TOMS ended after 2001). There are clear similarities among the various satellite data, all showing the highest AOD over land in dust and biomass burning regions in Africa, pollution regions in East China, and over ocean in the continental outflow areas. On the other hand, there are also obvious differences. For example, over land TOMS and MODIS show higher AOD in the western US than the eastern US, whereas SeaWiFS and MISR display the opposite. Over ocean, the annual average AOD is highest from MISR (0.160) and the lowest from SeaWiFS (0.104); AVHRR-GACP shows the strongest spatial gradient and TOMS shows the weakest due to its poorer detection sensitivity to "background" maritime aerosols (O. Torres, personal communication, 2013). Between the two AVHRR retrievals, AOD from CDR is generally lower than that from GACP in mid- to high latitudes but is higher in the tropics. There is a distinguishable AOD band in the Southern Ocean centered at about 60° S from AVHRR-GACP, MODIS-Terra, and MISR, which is much less visible from AVHRR-CDR and SeaWiFS (TOMS has little coverage beyond 45° S). Although a recent study has attributed this AOD band primarily to the contamination by stratocumulus and low broken cumulus clouds in the MODIS retrieval (Toth et al., 2013), the AOD over the Southern Ocean is expected to be higher than that over the tropical remote ocean mainly due to strong winds that drive higher sea salt and DMS emissions. Therefore, the band seen in AVHRR-GACP, MODIS-Terra, and MISR seems physically meaningful, although the magnitude is likely biased high because of cloud contamination and/or other artifacts suggested in recent studies (Zhang and Reid, 2010; Toth et al., 2013; Kalashnikova et al., 2013).

The model results (First panel, last row in Fig. 4) capture the high AOD over dust, pollution, and biomass burning regions and the transport of aerosols across the oceans. It also simulates an aerosol band in the Southern Ocean around 60° S, consistent with AVHRR-GACP, MISR, and MODIS, although the magnitude is lower than the satellite retrievals by 0.05 to 0.1, which would be more consistent with the new MODIS product (collection 6) with better detection of thin cirrus clouds and wind-speed correction, resulting in a 0.04–0.12 AOD reduction in the Southern Ocean (Levy et

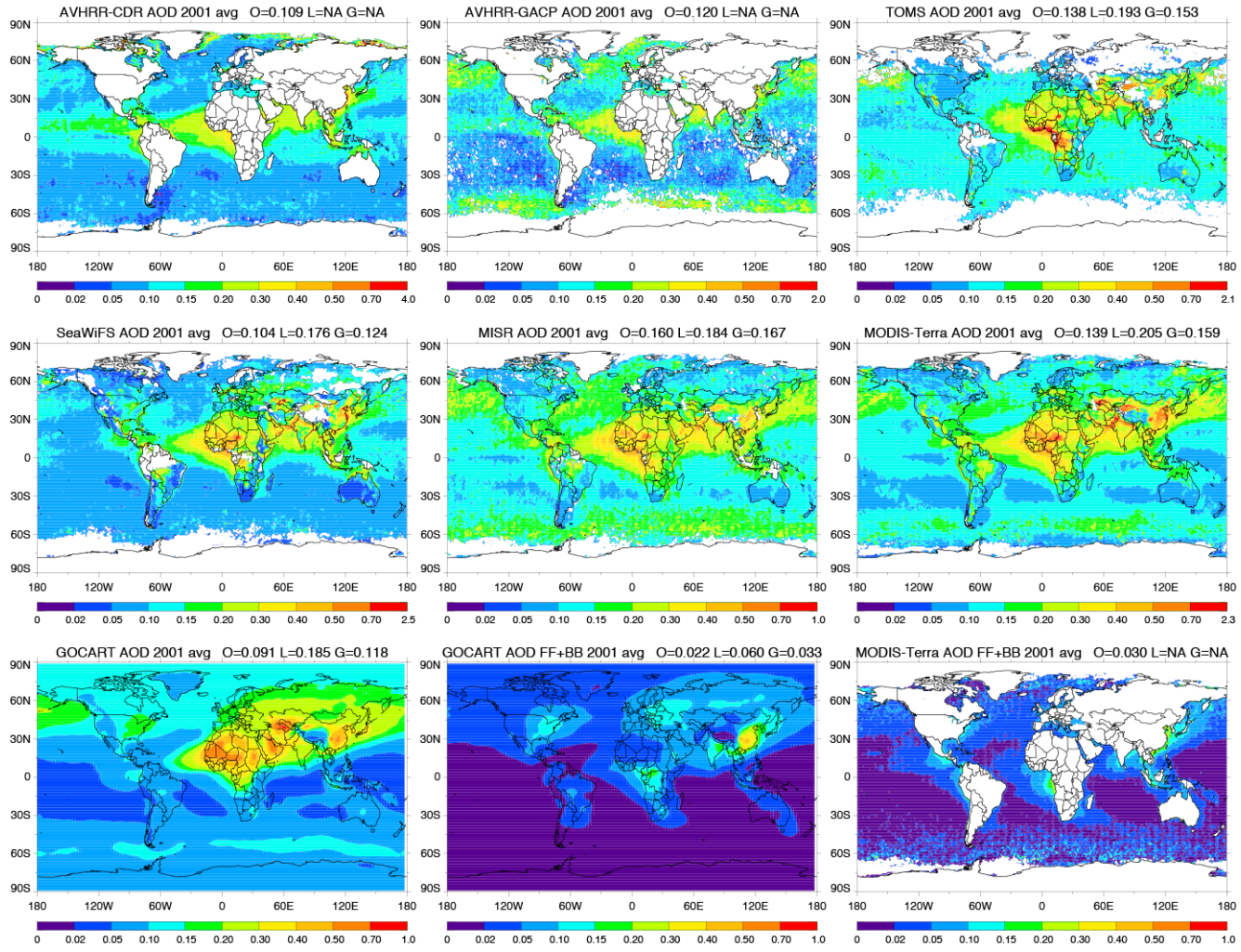

Fig. 4. Spatial distributions of 2001 annual average AOD from satellite retrieval products and GOCART model. From left to right, 1st row: AVHRR-CDR (left), AVHRR-GACP (middle), TOMS (right); 2nd row: SeaWiFS (left), MISR (middle), MODIS-Terra (right); 3rd row: GOCART-simulated total AOD (left) and FF+BB AOD (middle) and MODIS-derived FF+BB AOD (right). O, L, and G are for ocean, land, and global averages. White areas indicate no data. Annual average values over ocean (O), land (L), and globe (G) are shown on top of each panel (NA = not available) except the last one. These averages are obtained with the available data from each individual data set without matching their spatial availability, i.e., the area included in the average varies with data sets. (The color scale for the AOD panels is the same except the maximum values at the end of the highest color scale.)

al., 2013). In the tropical oceans the model is much lower than satellite products.

The last two panels in Fig. 4 display the AOD from combustion sources (fossil fuel/biofuel and biomass burning, noted as FF+BB) simulated by the model (middle panel) and estimated based on the MODIS data for 2001. The model results are obtained as the difference between the "standard" and "natural" simulations (see Sect. 2.3), and the MODIS-based estimate is derived empirically from the MODIS AOD and fine mode fraction, with corrections to exclude fine mode natural dust and marine aerosols (Kaufman et al., 2005; Yu et al., 2009). The MODIS-based results are only available over ocean. As expected, the model shows that the combustion AOD is mostly concentrated in the pollution and biomass burning source regions over land, but its influence is wide-spread, extending to the ocean in the Northern Hemisphere and the Arctic, especially over the immediate downwind regions from the continents. The MODIS-based combustion AOD over the ocean shows similar spatial patterns, with higher values over the continental outflow regions than over the open ocean; but it is higher than the model in the tropical ocean areas around Central America and Indonesia, which may be attributed in part to the volcanic aerosol in these areas (which is not considered in the Kaufman–Yu empirical method, see volcanic emission in Fig. S1), and/or to the model underestimation of tropical biomass burning

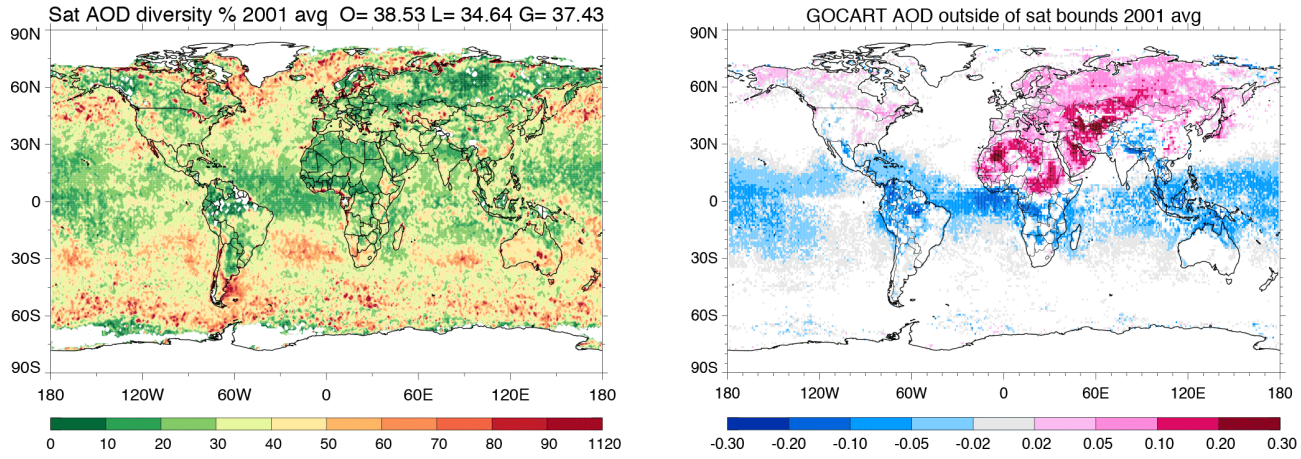

Fig. 5. (left) Satellite AOD diversity, defined as 1/2 ($AOD_{max} - AOD_{min}$) / $AOD_{median} \times 100\,\%$, for all available satellite annual mean AOD data points shown in Fig. 4, and (right) GOCART-simulated AOD that are outside of the satellite AOD range.

emissions (see next section). A relatively high combustion AOD band over the Southern Ocean in the MODIS-based product is most likely an artifact.

To further illuminate the differences among the satellite data and between model and multiple satellites, in Fig. 5 we show the "diversity" of satellite annual mean AOD in 2001 to reveal the degree of agreement among these data sets at different geographic locations (left panel), and the model results that are outside of the bounds of satellite data (right panel). Here the satellite diversity, expressed as percentage, is defined as 1/2 ($AOD_{max} - AOD_{min}$) / $AOD_{median} \times 100\,\%$ for all available satellite data points in each $1^\circ \times 1^\circ$ grid. Note that the availability of satellite data differs among the grid cells (maximum number of data points is 4 over land and 6 over ocean, See Fig. S2 for a map of available data points), but our purpose here is to show the consistency among the available data sets. Satellite data agree best over large deserts (Sahara, Middle East), major biomass burning areas (North Africa savanna, South America, Southeast Asia), northern boreal regions, Indo-Gangetic Plain, and tropical oceans where the diversity are mostly within 20–30 %, but they are apart over large ocean areas in the mid- to high latitudes and over land areas with elevated terrain (e.g., South China, Australia, Chile/southern Argentina, and part of the western US) where the diversity is higher than 50 %. There are also some "hot spots" mostly at high latitudes with extremely high diversity, where the satellite data should be considered highly uncertain.

In light of the diversity in the satellite data, we reveal the disagreement between model and multiple data sets in Fig. 5 (right panel) at location where the modeled AOD is outside of the range of the satellite AOD. The modeled AOD is higher than all satellite data over extended land areas in the Northern Hemisphere, particularly over the "dust belt" region from North Africa to Central Asia, but it is lower than the satellite data over the Tibetan Plateau and Indo-Gangetic Plain as well as in the tropical belt over both land and ocean. This geographic pattern of the model-data difference suggests that the dust in GOCART model is likely to be too high and the biomass burning in the tropical area is too low.

Overall, the GOCART model generally follows the observed patterns for both total and combustion AOD, but falls outside and below the range of the observations in the region dominated by tropical biomass burning and in the tropical oceans, and outside and above the range in dust-dominated regions. Such differences point out the direction for future model improvements, but they do not necessarily compromise the trend analysis in this study.

4.2 Multi-decadal aerosol variations over land regions

4.2.1 AOD in pollution, dust, and biomass burning regions

To investigate regional trends, we first compare the AOD time series from satellite retrievals and model simulations over different land regions. Among the regions listed in Table 1 (displayed in Fig. 1), we focus our comparisons here on 10 selected land regions, including 4 major pollution source regions of USA, EUR, EAS, and SAS (note that EAS and SAS are also dust source regions) and 2 biomass burning regions of SAM and SEA in Fig. 6a, and 4 dust source regions of SHR, SHL, MDE, and CAS in Fig. 6b (comparisons of all 15 land regions are shown in the Supplement, Fig. S3a). Model-estimated AOD speciation (color-coded, vertically stacked bars) and the combustion (FF+BB) AOD (red bars next to the aerosol speciation) are indicated in Fig. 6. The regional average AOD for each data set is calculated from the available data within the region independently; i.e., spatial and temporal matching of the different data sets and the model is not imposed, not only because there is very limited common coverage, but also because the purpose here

is to examine the trends with each data set independently. Although such averaging can introduce differences between data sets simply because of their different spatial and/or temporal sampling, the regional trends should be relatively robust, provided the available data are representative.

The only satellite data set available over land before the EOS era is TOMS; however, as described earlier, it suffers from coarse spatial resolution and the lack of onboard cloud screening capability that limit retrieval availability and data quality. A strict cloud-free pixel standard has been applied to minimize cloud contamination in the TOMS AOD product, which also removes high-AOD pixels (e.g., volcanic aerosol signals from El Chichón and Pinatubo are mostly screened out) such that the averaged AOD from the remaining pixels can be significantly biased. Because of the limitations, TOMS data is used mainly for trend assessment rather than for their absolute AOD values (it is included in Fig. 6 for informational purposes). This limits the available satellite observations over land only within the last decade or so, that is, after 1997, with SeaWiFS, MISR, and MODIS.

Figure 6 shows that the most pronounced feature during the 30-year time period from the model is the worldwide influence of large volcanic eruptions, that is, El Chichón in 1982 and Pinatubo in 1991. Sulfate aerosols formed from these eruptions can last for several years. For the periods lacking major volcanic influence (i.e., in the mid- to late 1980s and in the 2000s), Fig. 6a displays a decreasing AOD trend over the pollution source regions of USA and EUR, and the model shows that such a decrease is mostly driven by the decline of combustion AOD (red bars), in line with the fossil fuel/biofuel emission reduction trends in these regions (Fig. 2). The reduction over EUR is particularly remarkable: the total and combustion AOD in the late 2000s are only about half and one-third of their corresponding values in the early 1980s from the model. In contrast, over EAS and SAS the combustion AOD has increased significantly by 40 % and 120 %, respectively, for the same period of time. However, the overall increase of total AOD is less than 20 % in EAS and SAS, because of the relatively large amount of dust aerosols in these regions that either have negligible trend (in EAS) or a decreasing trend (in SAS) to mask the increasing trend of the combustion AOD. Compared with satellite AOD from SeaWiFS, MISR, and two MODIS products from the late 1990s to late 2000s, the model-simulated AOD agree with satellite data within 0.02–0.05 over USA and EUR, where the satellite data are also consistent with each other. Over EAS and SAS, AOD from SeaWiFS and MISR are usually 0.05–0.08 lower than the two MODIS products, and the model simulations agree better with SeaWiFS and MISR although the model is still about 0.05–0.08 lower than these two satellite data over SAS.

For regions that are mainly influenced by biomass burning (i.e., SAM and SEA; bottom row in Fig. 6a), there are considerable interannual variations but not obvious trends. The model captures the interannual variability observed by SeaWiFS, MISR, and MODIS in the last decade but the simulated AODs are a factor of two lower than that from satellite retrievals. Considering that the GOCART model had much smaller bias (within 20 %) in our previous simulations using higher biomass burning emission factors (Chin et al., 2009), we suggest that the A2-ACCMIP biomass burning emission for the aerosol species, which is based on the Global Fire Emission Dataset (GFED) version 2 for the period of 1997–2008 (Granier et al., 2011; Diehl et al., 2012), is likely too low (see also biomass burning emission comparisons in Petrenko et al., 2012).

Over the dust source regions of SHR, SHL, MDE, and CAS, AOD from the model tends to be higher than that from the satellite retrievals (other than TOMS) by 0.05 to 0.15 (Fig. 6b), which is likely the result of the model overestimating dust emissions. The model shows a clear increase of dust in SHL in the early 1980s, and then a leveling-off or a decrease since then. The model shows an increase of dust AOD in SHR during the mid- to late 2000s, in line with SeaWiFS but not with MISR and MODIS. Over MDE, both model and satellite data suggest an increasing AOD tendency in the last 10 years, driven by the increase of dust, which is consistent with prior SeaWiFS and AERONET data analyses in that region (Hsu et al., 2012). In CAS, the model-simulated dust AOD has increased by 0.04–0.05 from 1980 to 2009, although AOD from combustion sources (red vertical bars) has decreased by 0.04 over the same time period, offsetting the dust AOD increase. The model-simulated interannual variability in the 2000s is stronger and AOD is much higher than SeaWiFS and MISR over CAS but agrees better with MODIS, even though the simulated AOD is still 0.1–0.15 higher than MODIS.

Given some discrepancies between satellite data and model, we further evaluate the model-simulated AOD with the ground-based sun photometer data from the AERONET measurements in different regions. As we mentioned earlier (Sect. 3.2), most AERONET measurements started in the 2000s and only 15 sites have data for at least 12 years (Fig. 3). We show in Fig. 7 the monthly AOD from 1995 to 2009 from AERONET and GOCART simulation at five AERONET sites over land for their relatively long-term record and under different aerosol regimes: GSFC in the US and Lille in France, dominated by combustion-generated aerosols; Alta Floresta in the Amazon, dominated by biomass burning aerosols during the burning season; and Sede Boker in Israel and Banizoumbou in Niger, dominated by dust. The only island site from AERONET with data started in the 1990s is Cape Verde off the west coast of North Africa, which receives dust from the upwind Sahara and Sahel all year long. AOD from AERONET and GOCART over Cape Verde are also shown in Fig. 7 (results for the rest of the long-term sites are shown in Fig. S4 and the overall model-AERONET comparison statistics listed in Table S1). Satellite AOD data over each site are also plotted for comparisons. To better reveal the temporal trends, the annual averaged relative

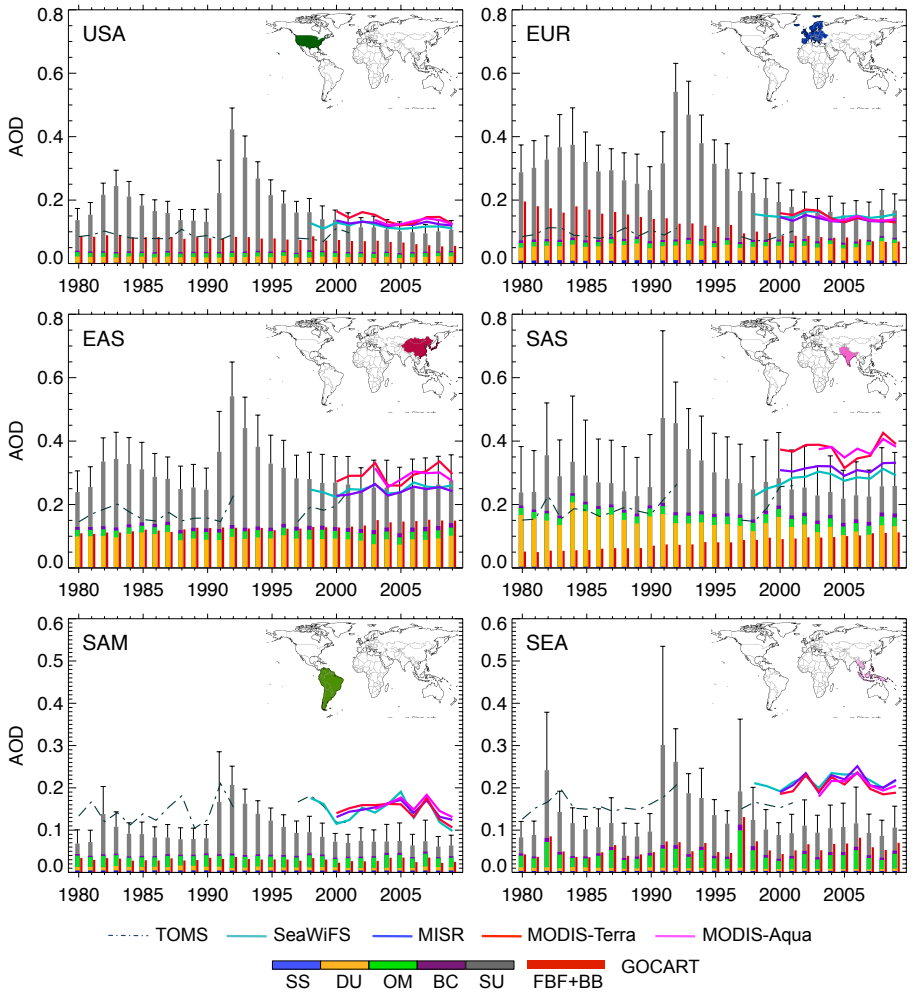

Fig. 6a. Regional annual average AOD from 1980 to 2009 in four pollution source regions of USA, EUR, EAS, and SAS. Region domains are shown in each panel (also in Fig. 1). Satellite retrievals are presented in continuous color lines, and GOCART results are displayed in vertically stacked color bars showing AOD composition (SS = sea salt, DU = dust, OM = organic matter, BC = black carbon, and SU = sulfate). AOD from fossil fuel and biomass burning (FF+BB) sources is shown in red vertical lines next to the aerosol composition. All products are averaged within the region domains without considering coincidental spatial/temporal coverage. Note that there is no AVHRR retrieval available over land. Standard deviation of monthly average of regional AOD from GOCART is shown in thin black vertical lines (for clarity, only positive part is plotted and the deviation from satellite data is not displayed).

AOD anomaly is expressed in the right column of Fig. 7 as the ratio of the annual AOD to the 2000–2001 average (2000–2001 is a common period when multiple data sets are available). The model shows a general decrease of AOD at GSFC and Lille, large interannual variability over Alta Floresta with no overall trend, and a small increase over Sede Boker and Banizoumbou since 2000. These changes are in the same direction as AERONET data except at Lille, where AERONET data indicate no decrease since the late 1990s. On average, the model agrees with AERONET AOD within 15–20 % over GSFC, Lille, Banizoumbou, and Cape Verde ($B = 0.87$–1.20), but overestimates the AOD at Sede Boker by nearly 50 % ($B = 1.48$) and underestimates that at Alta Floresta by 60 % ($B = 0.38$). The temporal trends/variations and model bias at these AERONET sites are consistent with the behavior of model-satellite comparisons for the corresponding regional averages in Fig. 6, although it is clear from Fig. 7 that satellite AODs are too high over Lille, Sede Boker, and Cape Verde. Interestingly, the direction of changes is different between Banizoumbou near the dust source and Cape Verde downwind in the 2000s: AOD over Banizoumbou (in SHL) shows an increasing tendency (except MODIS-Terra), especially from AERONET, whereas over Cape Verde (in CAT) no such increase appears. These AOD changes seem to be representative of the corresponding regional behaviors (SHL in Fig. 6 and CAT in Fig. 9) for the same time periods.

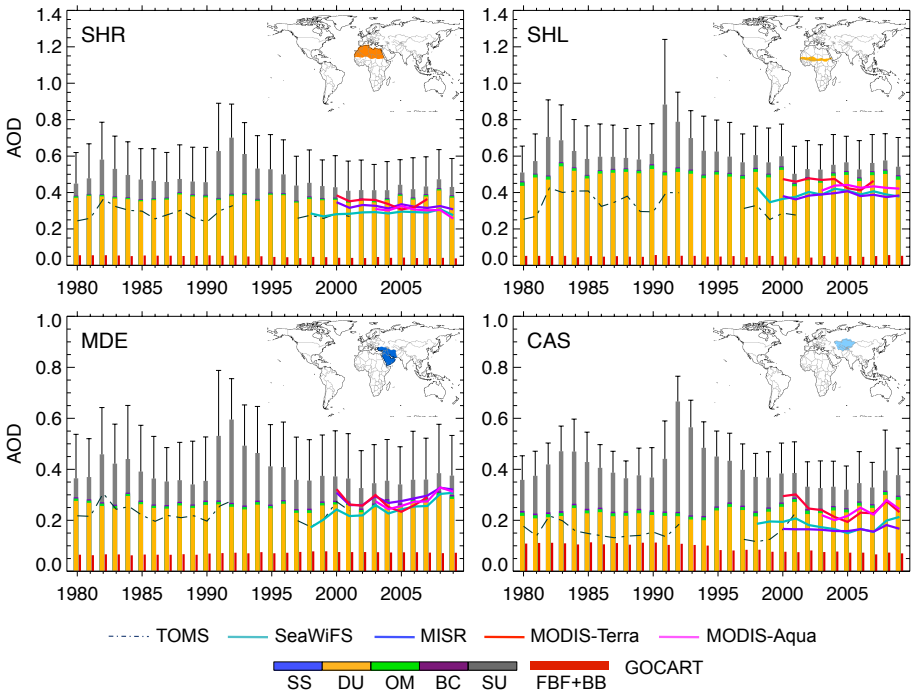

Fig. 6b. Same as Fig. 6a but for four dust source regions of SHR, SHL, MDE, and CAS.

4.2.2 Aerosol surface concentrations over the US, Europe, and the Arctic

Complementary to the remotely sensed AOD data (an optical measurements of the atmospheric column which does not distinguish aerosol species), the ground-based in situ measurements provide mass concentrations of different aerosol species and their precursor gases, offering another aspect in assessing the multi-decadal aerosol trends and evaluating the model, especially in the Arctic where the polar-orbiting satellites have very little coverage. However, as shown in Fig. 3, the long-term concentration measurements over land are mostly limited to locations in North America and Europe. Figures 8a–c compare model-simulated aerosol species concentrations with measurements at selected surface sites in the US, Europe, and the Arctic, respectively, demonstrating the concentration change at different locations.

Over the US: Fig. 8a shows monthly concentrations and interannual variability of sulfate, BC (or elemental carbon, EC, in IMPROVE), OC, and fine mode dust concentrations at two IMPROVE sites from 1988 to 2007: a remote site in the San Gorgonio Wilderness at 1.7 km elevation in southwestern US (southern California), and an urban site in Washington DC in the eastern US near sea level. These two sites are chosen to represent contrasting environments and geographic locations. Concentrations of sulfate, BC, and OC over San Gorgonio are significantly lower than those over more polluted Washington DC from both model and observations but dust is higher due to its near-desert location. Both observation and model show decreasing trends of sulfate, BC, and OC at these two sites (30–40 %, right column), mostly echoing the reduction of anthropogenic emissions over the US during the time period, although the trends are smoother and the degree of decline is much lower for BC and OC in the model. On the other hand, dust concentrations fluctuate from year to year with little trend. At San Gorgonio all species show repetitive seasonal cycles that are captured by the model, but at Washington DC only sulfate has a clearly defined seasonal pattern while other species display a much less organized temporal variation that is not reproduced by the model. The largest disagreement between the IMPROVE data and the model is in the BC and OC concentrations that are 40–70 % too low in the model. Such misrepresentation can be attributed largely to the underestimation of fossil fuel combustion and biomass burning emissions (e.g., Park et al., 2004) and the unaccounted sources (e.g., local emission, inadequate secondary organic aerosol formation) in the model. The reduction of pollutant level is common among the 44 long-term IMPROVE sites over the US (Fig. 3) with an average value of about 40 % (illustrated in Fig. S5 for sulfate).

Over Europe: the long-term measurements of aerosol and related species in the EMEP network began in the late 1970s to measure the "acidifying" compounds. Measurements of other species such as BC and OC started much later, mostly in the 2000s. Therefore in this study we use the sulfur data from EMEP, including sulfate aerosol and SO_2 gas (which is the precursor compound for sulfate. Fig. 8b shows the long-term data at two EMEP sites, Tange in Denmark and Chopok

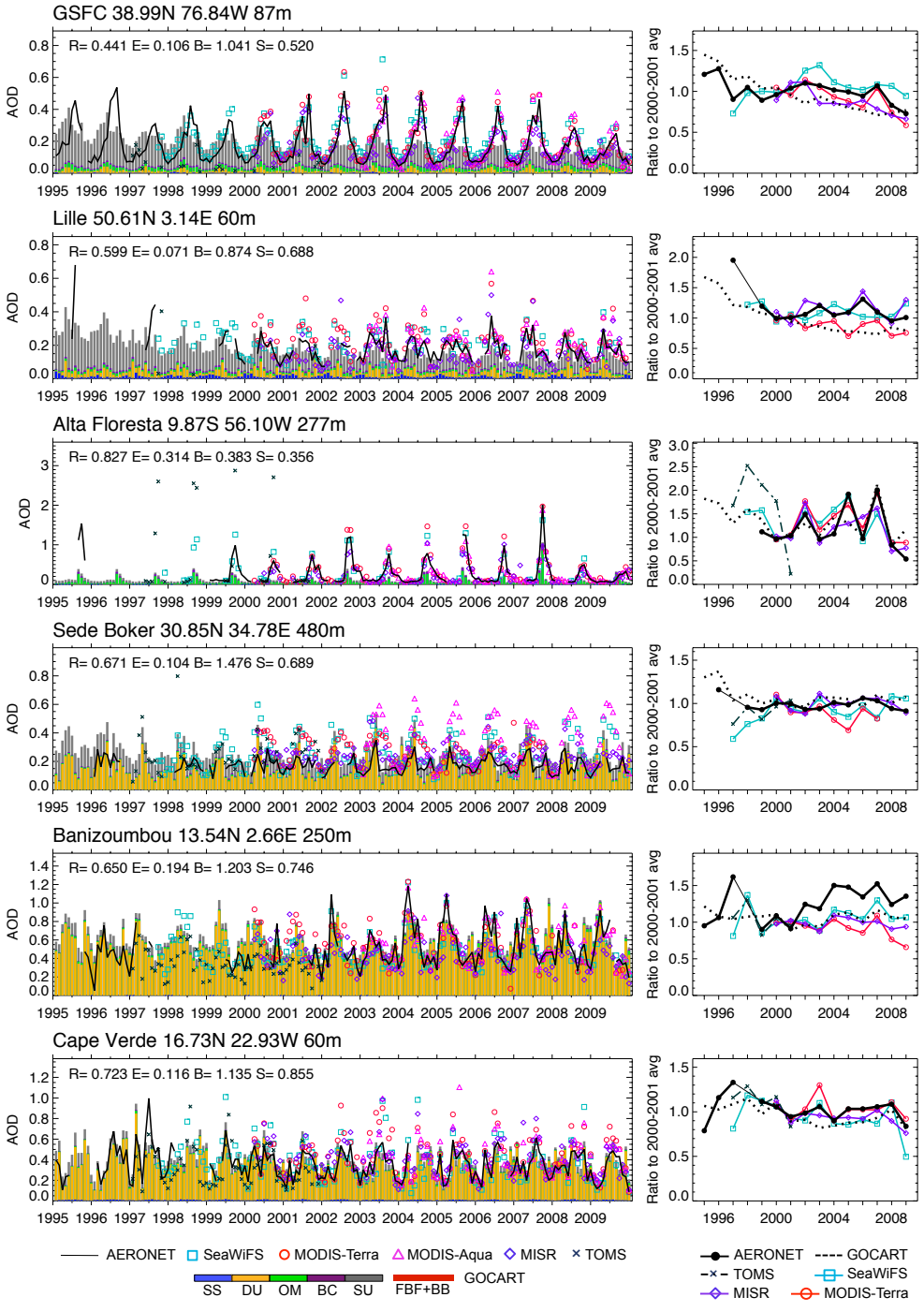

Fig. 7. Left column: monthly AOD from 1995 to 2009 at five AERONET continental land sites, GSFC in eastern USA, Lille in France, Alta Floresta in the Amazon, Sede Boker in Israel, and Banizoumbou in the Sahel. AOD at the Cape Verde site off the west coast of North Africa is also shown (last row). Statistical measures of comparisons between observations and GOCART are shown on each panel: R = correlation coefficient, E = root mean square error, B = mean bias (model/observation), and S = skill score (Taylor, 2001). Right column: ratio of annual mean AOD to the 2000–2001 average at corresponding sites, showing the interannual variability/trend over the 15-year period with the AERONET data in black solid, satellite observations in colored solid, and model in dotted black lines. Thin solid black line in the right column connects the points with missing year(s) in between for visual continuity.

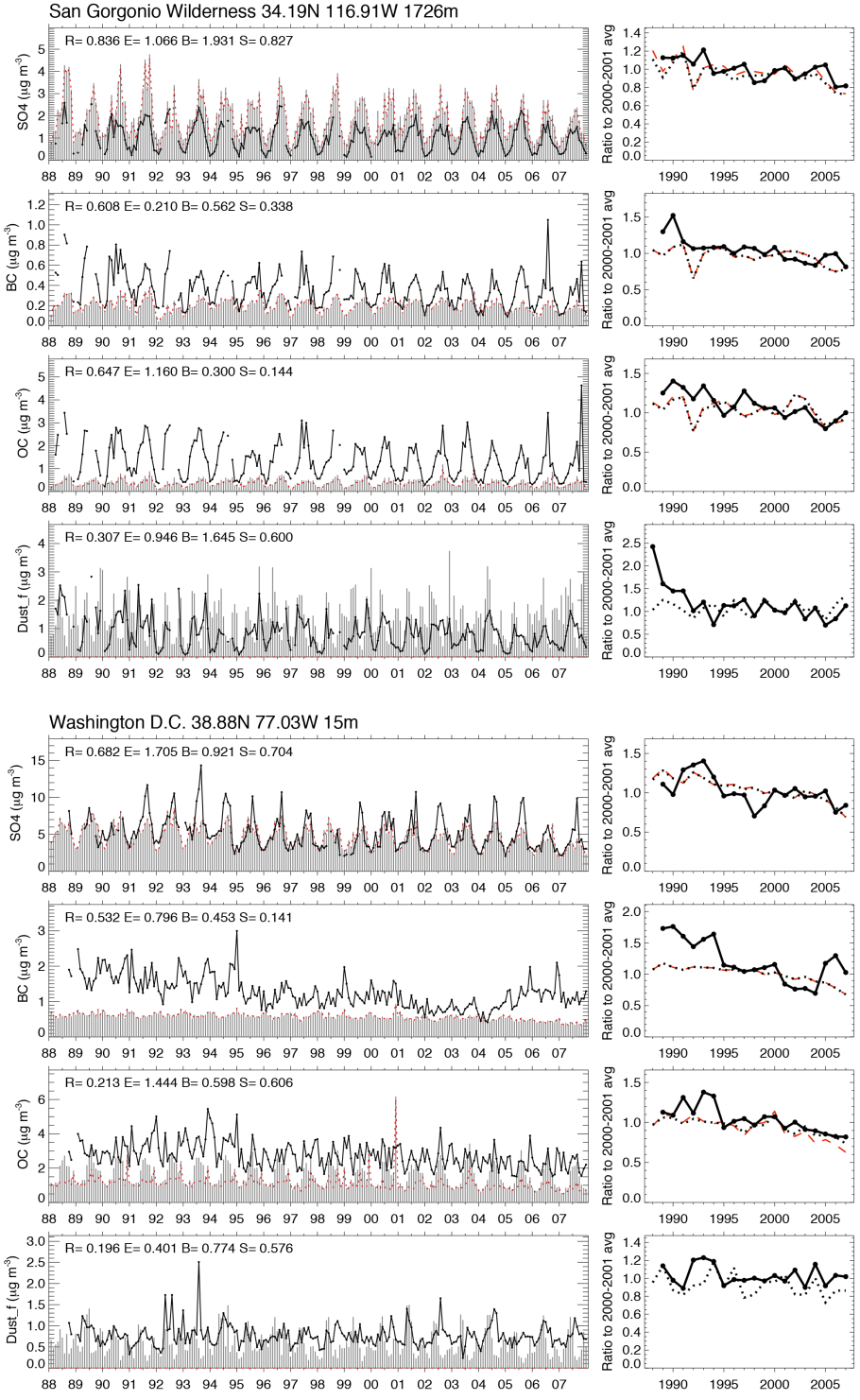

Fig. 8a. Left column: monthly averaged surface concentrations (μg m^{-3}) of sulfate, BC, OC, and fine mode dust from 1988 to 2007 at two US sites, San Gorgonio Wilderness in California, western US (top four rows) and Washington DC, eastern US (bottom four rows). Data from the IMPROVE network. Observations are shown in black lines and the model results in grey bars for total amount and dotted red lines for FF+BB amount. Statistical measures (R, E, B, and S) are defined as the same as in the Fig. 7 caption. Right column: ratio of annual mean concentrations to the 2000–2001 average at corresponding sites, showing the interannual variability/trend over the 20-year period with the observation and models in solid and dotted lines, respectively. Thin solid black line in the right column connects the points with missing year(s) in between for visual continuity.

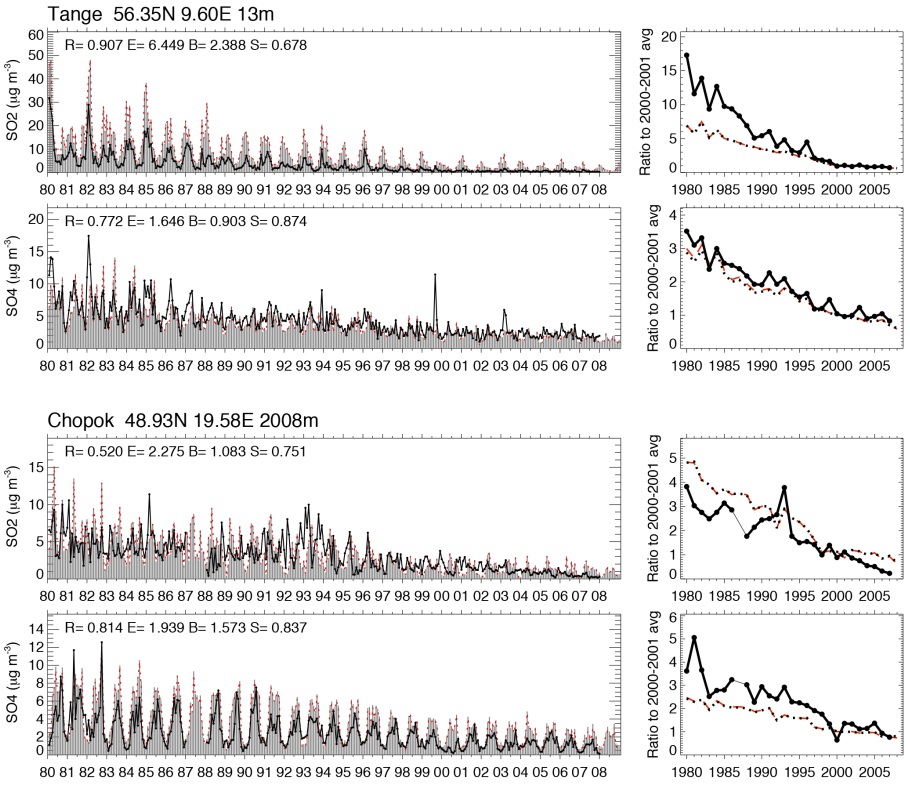

Fig. 8b. Left column: monthly averaged surface SO_2 and sulfate concentrations ($\mu g\,m^{-3}$) from 1980 to 2008 at two European sites, Tange in Denmark (top two rows) and Chopok in Slovakia (bottom two rows). Data from the EMEP network. Observations are shown in black lines and the model results in grey bars for total amount and dotted red lines for FF+BB amount. Statistical measures (R, E, B, and S) are defined as the same as in Fig. 7 caption. Right column: corresponding ratio of annual mean concentrations to the 2000–2001 average showing the interannual variability/trend over the 20-year period with the observation and models in solid and dotted lines, respectively. Thin solid black line in the right column connects the points with missing year(s) in between for visual continuity.

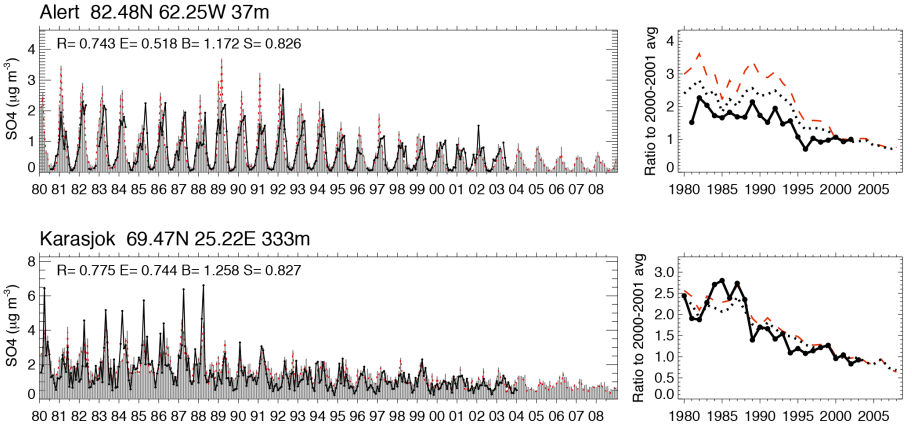

Fig. 8c. Left column: monthly averaged surface sulfate concentration ($\mu g\,m^{-3}$) from 1980 to 2008 at two Arctic sites, Alert, Canada in the western Arctic (top row) and Karasjok, Norway in the eastern Arctic (bottom row). Data provided by P. K. Quinn. Observations are shown in black lines and the model results in grey bars for total amount and dotted red lines for FF+BB amount. Statistical measures (R, E, B, and S) are defined as the same as in the Fig. 7 caption. Right column: corresponding ratio of annual mean concentrations to the 2000–2001 average showing the interannual variability/trend over the 20-year period with the observation and models in solid and dotted lines, respectively.

in Slovakia. These two sites are chosen as examples showing the sulfur concentration changes in different geopolitical regions and at different altitudes. The decrease of SO_2 and sulfate concentrations is remarkable in the past three decades over these sites. EMEP data show a factor of 16–18 reduction of SO_2 at both sites and a lesser degree of sulfate with factors of about 9 and 4 at Tange and Chopok, respectively. The model also shows a large drop in SO_2 and sulfate concentrations, but with smaller magnitudes, by a factor of 6–7 for SO_2 and 3–4 for sulfate. The weaker declining trend of sulfate as compared with SO_2 can be explained mostly by the limiting factor of the availability of the oxidants (OH, H_2O_2) near the pollution source (Chin et al., 1996, 2000; Koch et al., 1999) needed to convert SO_2 to sulfate, such that the sulfate amount is less sensitive than SO_2 concentration to the SO_2 emission change. The decrease of the sulfur concentration is widespread over Europe, as seen at the 64 long-term EMEP sites (Fig. 3), and is almost entirely due to the drastic decline in SO_2 emissions (illustrated in Fig. S5 for sulfate).

Over the Arctic: Fig. 8c shows the surface sulfate concentrations at two sites inside the Arctic Circle: Alert in Canada, located in the western Arctic, and Karasjok in Norway, located in the eastern Arctic (Fig. 3). These two sites are chosen not only for their different geographical locations in the Arctic but also for their long-term data record. Because of the remoteness of these sites, sulfate there is mostly transported from mid-latitude polluted areas, especially from Europe (e.g., Shaw and Stamnes, 1980; Rahn, 1981; Chin et al., 2007; Shindell et al., 2008). Similar to Europe, sulfate concentrations at these Arctic sites also display a significant decrease such that the concentrations in the 2000s are two- to threefold lower than the earlier values in the 1980s.

By separating combustion-generated aerosol species from the natural ones (dust, biogenic, and volcanic), the model shows that sulfate at the land sites is mostly from the combustion sources (red lines in Fig. 8), BC is entirely from the combustion sources, whereas a sizable fraction of OM can come from natural sources (biogenic secondary organic aerosol) depending on the locations (such as at WASH1 in Fig. 8a). The large volcanic eruptions that exerted profound enhancements of sulfate AOD globally show little effect on surface sulfate concentrations.

4.3 Multi-decadal variations of aerosols over ocean regions

4.3.1 AOD in continental outflow and remote ocean regions

We compare the AOD from satellite retrievals and model simulations over the ocean in six oceanic areas (Fig. 9), five of which (NAT, WNP, CAT, NIN, and SAT) are influenced by the continental outflow of pollution, dust, and biomass burning, and one (SOU) is in the remote area in the Southern Ocean (comparisons for all 12 ocean regions are shown in the Supplement, Fig. S3b). Aerosols from the El Chichón and Pinatubo volcanic eruptions are again the most distinct features in the long-term AOD record from both AVHRR retrievals and GOCART simulations. The AVHRR data show comparable maximum AOD values between El Chichón and Pinatubo over the northern hemispheric oceans, whereas GOCART generates a higher AOD from Pinatubo than from El Chichón. In the time periods with little influence from major volcanic eruptions, the most clear regional changes from the mid-1980s to 2000s over the continental outflow regions are the declining trends in NAT and CAT (about 20 %), due to the reduction of anthropogenic and dust influences from the neighboring continents. On the other hand, there is an increasing trend (15 %) over WNP consistent with the increasing combustion aerosol transport from EAS between the mid-1980s and 2000s, but the model suggests that the anthropogenic AOD increase over NIN is damped by a decrease in dust AOD, similar to the changes in SAS. Thus there is little trend for NIN overall in the non-volcanic period during the past three decades, although satellite data indicate an increasing trend in the 2000s. The model matches the two AVHRR and SeaWiFS retrievals within 0.02–0.03 over NAT, CAT, and WNP, but it is about 0.02–0.08 lower than MISR and MODIS in the same regions. The model is also consistent with the AVHRR-GACP over NIN but it is 0.05–0.1 lower than other satellites.

Over SAT, GOCART simulations indicate that biomass burning aerosol, transported mainly from the upwind continents, is more influential here than over other regions. However, the model is significantly lower than all satellite products by 0.05–0.10 for most years. Although the underestimation could be attributed in part to the low biomass burning emissions (also shown in Fig. 6b), a general large underestimation of AOD by the model over much of the tropical and subtropical ocean suggests that the model may have missed or underestimated some aerosol sources over these ocean regions. It is possible that sea salt emission in the tropics might be too low (Jaeglé et al., 2011), sulfate chemical production could be too slow (Yu et al., 2009), or primary organic matter emissions (Gantt et al., 2011) that should be included in the model. However, higher sea salt production seems unlikely, based on the comparisons with the surface measurements over the tropical/subtropical area (see next section). On the other hand, satellite AOD may exhibit a high bias over the ocean, which could be caused by contributions from unscreened cloud or unaccounted-for whitecaps (e.g., Mishchenko et al., 1999; Kahn et al., 2007). A high bias is found in comparisons between satellite data and shipboard measurements (Smirnov et al., 2011), which is reduced when newer algorithms are applied to the input data (Zhang and Reid, 2006, 2010; Levy et al., 2013).

In SOU between 45° S and 66.5° S, AOD values from GOCART, AVHRR-CDR, and SeaWiFS are close to each other, but they are much lower than other satellite products. As noted earlier (Sect. 4.1), further removal of thin-cirrus cloud

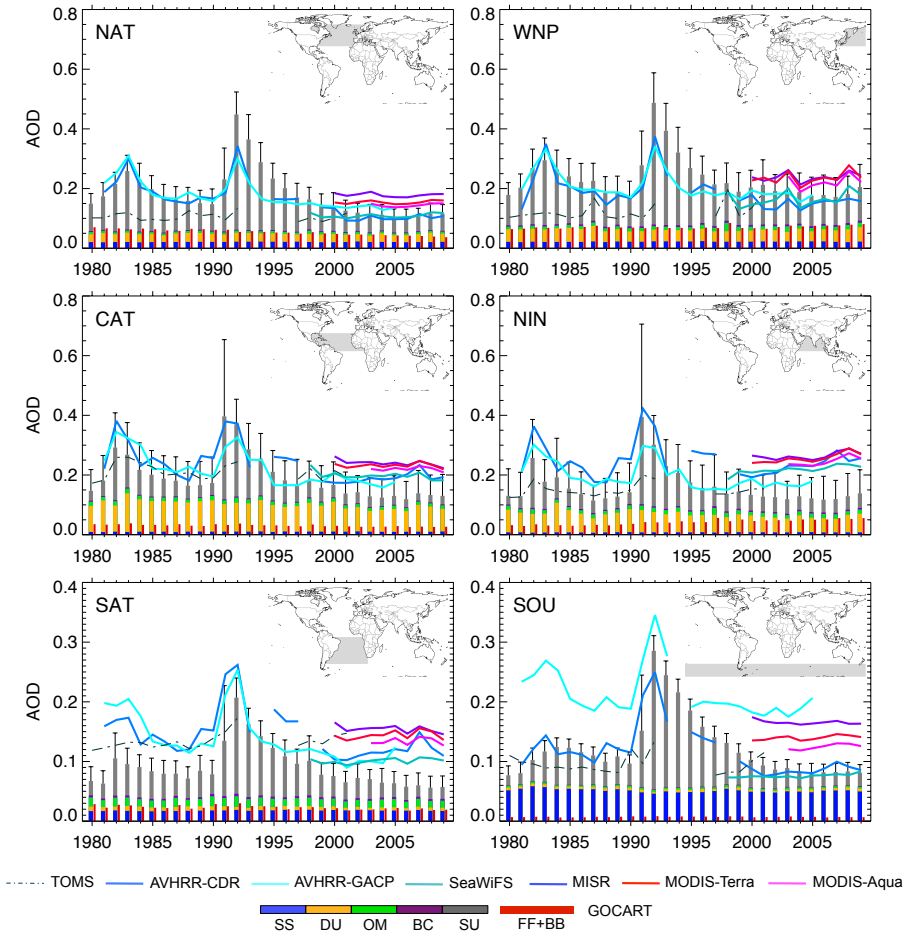

Fig. 9. Same as Fig. 6a but for six ocean regions of NAT, CAT, SAT, WNP, NIN, and SOU (domains shaded in grey). AVHRR retrievals are available over ocean.

contamination and correction for wind-speed-dependent surface reflectance would bring the MODIS AOD down by 0.04–0.12 in this region (Levy et al., 2013), which would be much closer to AVHRR-CDR, SeaWiFS, and GOCART. The model suggests that about 20–25 % of AOD over SOU is contributed by sulfate formed via DMS-SO_2 oxidation (indicated by SU in SOU region in time periods without large volcanic influences), as was also shown in our previous model studies (Chin et al., 2000, 2002, 2009).

Interestingly, GOCART indicates that the sea salt is not the major component for column AOD over much of the ocean, except in SOU (also see Fig. S3b), even during the time periods without influences from El Chichón or Pinatubo: pollution and dust transport constitute more than half the AOD over the northern hemispheric mid-latitude oceans and the Indian Ocean, whereas biomass burning and natural aerosols (volcanic, DMS oxidation) influence the AOD in the tropical and subtropical areas.

4.3.2 Aerosol concentrations over oceanic island sites

Surface aerosol concentrations at about 30 island or coastal sites from the University of Miami network are available starting in the 1980s, but there are significant data gaps for some species and most sites have been inactive since the 1990s or early 2000s; only 5 sites have long-term (> 15 years) data coverage (Fig. 3) for at least one aerosol species and only Barbados and the University of Miami sites have data continuing to the end of 2009. The longest data record is the dust concentration at Barbados (measurements starting in the 1960s) (Prospero and Lamb, 2003). We show in Fig. 10a the surface concentrations of sulfate, dust, and sea salt at the Barbados and Miami sites, in Fig. 10b the same species at Midway Island in the Pacific, and in Fig. 10c sulfate, MSA, and sea salt at the Mawson Station on the coast of Antarctica. (Note that the sulfate term used here is for "non-sea-salt sulfate.") These sites are chosen for their longer or more complete coverage than other sites and for their diverse geographic locations (Atlantic, Pacific, near Antarctica). Data at other long-term island sites, American Samoa

from University of Miami measurements and at Mauna Loa from University of Hawaii, are shown in Fig. S6.

Dust at Barbados and Miami is predominantly from the trans-Atlantic transport from North Africa, whereas sulfate and sea salt are mostly from local or regional sources. Being further away from the North American continent and closer to the transported dust plume, Barbados is much less influenced by anthropogenic sulfate from North America, but receives much more dust from North Africa than Miami (Fig. 10a). The model shows a decreasing trend of sulfate at both sites with a larger magnitude at Miami (about 20 % and 40 % at Barbados and Miami, respectively), mostly due to the decrease of anthropogenic sulfate from North America. Sea salt does not seem to show a general trend at either site (the apparent increase from 1985 to 2000 in the Barbados data is attributed to the change of measurement method, J. Prospero, personal communication). On the other hand, the model indicates an overall 50–60 % decrease in dust concentration at Barbados from the early 1980s to the late 2000s, consistent with the Barbados data. Although the data at the Miami site are not conclusive for such a decreasing trend because of the relatively shorter data record, the model indicates a decreasing trend in the 1980s. This indication seems credible, given that the model closely reproduces the interannual variations of dust from 1989 to 2009 at Miami. Dust at both sites has a systematic seasonal variation, with a distinctive summer peak, but at Barbados the shape of seasonal variation is much broader than that at Miami. At Barbados dust starts to increase in early spring and gradually decays after summer, as determined by the seasonal intensity of dust activity in North Africa. On the other hand, at Miami dust increases sharply in July and diminishes quickly thereafter; this is caused by the seasonal variation of the transported plume, which shifts more to the north in the summer (e.g., Remer et al., 2008; Hsu et al., 2012) to reach Miami.

Midway Island in the middle of the North Pacific receives pollution and dust transported mostly from Asia (e.g., Prospero et al., 1999; Prospero et al., 2003; Chin et al., 2007). The data record for Midway ended in the early 2000s. Both model and data show seasonal and interannual variations of sulfate, dust, and sea salt at Midway with no evident trends (Fig. 10b). The model overestimates dust concentrations in Midway by a factor of 5, suggesting that the model may significantly overestimate the dust source in Asia and/or the dust trans-Pacific transport efficiency, although additional verification is necessary.

At the Mawson Station on the Antarctic coast, land-originated aerosols have little influence (Fig. 10c). Although the data record at Mawson is too short (< 10 years) to derive a trend, it reveals sulfur chemistry in the remote environment (Prospero et al., 1991; Savoie et al., 1992). The source of natural sulfate at Mawson is the photochemical oxidation of DMS, producing SO_2 and consequently sulfate. A branch of the DMS oxidation pathway also produces another natural aerosol species, MSA. Both sulfate and MSA have large, smooth seasonal cycles with peaks in the southern hemisphere summer, reflecting the seasonal cycles of ocean primary productivity and atmospheric photochemical processes, both of which are strongest in the summer. The model agrees with sulfate and MSA observations within 30 % and 18 %, respectively, suggesting that the biogenic sulfur cycle over the high latitude Southern Ocean area is well represented in the model.

4.4 Global patterns of AOD change

Due to the interannual variability of meteorology and significant perturbations from sporadic events, it is not always appropriate to deduce linear trend from the 30-year AOD record. It is also not assured that AOD changes over 30 years are linear, or even monotonic, in all regions. Here, we examine the differences between the beginning and end of two time segments, (1) the end of 1980s (1988–1989) to early 2000s (2000–2001), and (2) the early 2000s (2000–2001) to late 2000s (2008–2009), to identify geographic patterns of AOD changes during these two periods. The time segments were chosen to minimize large volcanic influences, to maintain close to normal climate conditions (i.e., near-neutral El Niño–Southern Oscillation index after averaging over 2 years), and to optimize the use of multiple satellite data sets that cover different time periods (see Table 3 and Fig. S7). In the first time segment, available satellite data include AVHRR-CDR, AVHRR-GACP, and TOMS whereas in the second time segment AVHRR-CDR, SeaWiFS, MISR, and MODIS-Terra are available. Difference maps are shown in Fig. 11a and 11b, respectively, for the two time segments. Although a 2-year period seems relatively short, such that the difference between the beginning and end of a time segment could reflect interannual variability rather than a decadal trend, such spatial difference maps together with the regional time series in Figs. 6 and 9 do provide complementary information about decadal-scale variations.

During the first time segment (Fig. 11a), both AVHRR products (first two panels in the left column) show a widespread AOD decrease over the ocean from the end of the 1980s (1988–1989) to the beginning of the current century (2000–2001), except in coastal areas of the Indian subcontinent, North Pacific mid-latitudes, and tropical African west coast. The GACP product also shows pockets of increase over the Southern Ocean. In contrast, TOMS (bottom panel, left column) presents a general AOD increase over the global oceanic area, except some areas over the Atlantic. However, the increase (0.02–0.05) is well within the range of the relatively large uncertainties in TOMS AOD (see Sect. 3.1), and hence the apparent trend is not conclusive. All satellite products show a clear AOD decrease off the west coast of North Africa and Angola but an increase in the tropics over the Gulf of Guinea. AOD changes near coastal regions usually directly reflect aerosol sources changes in the upwind land regions. For example, TOMS shows an AOD increase over

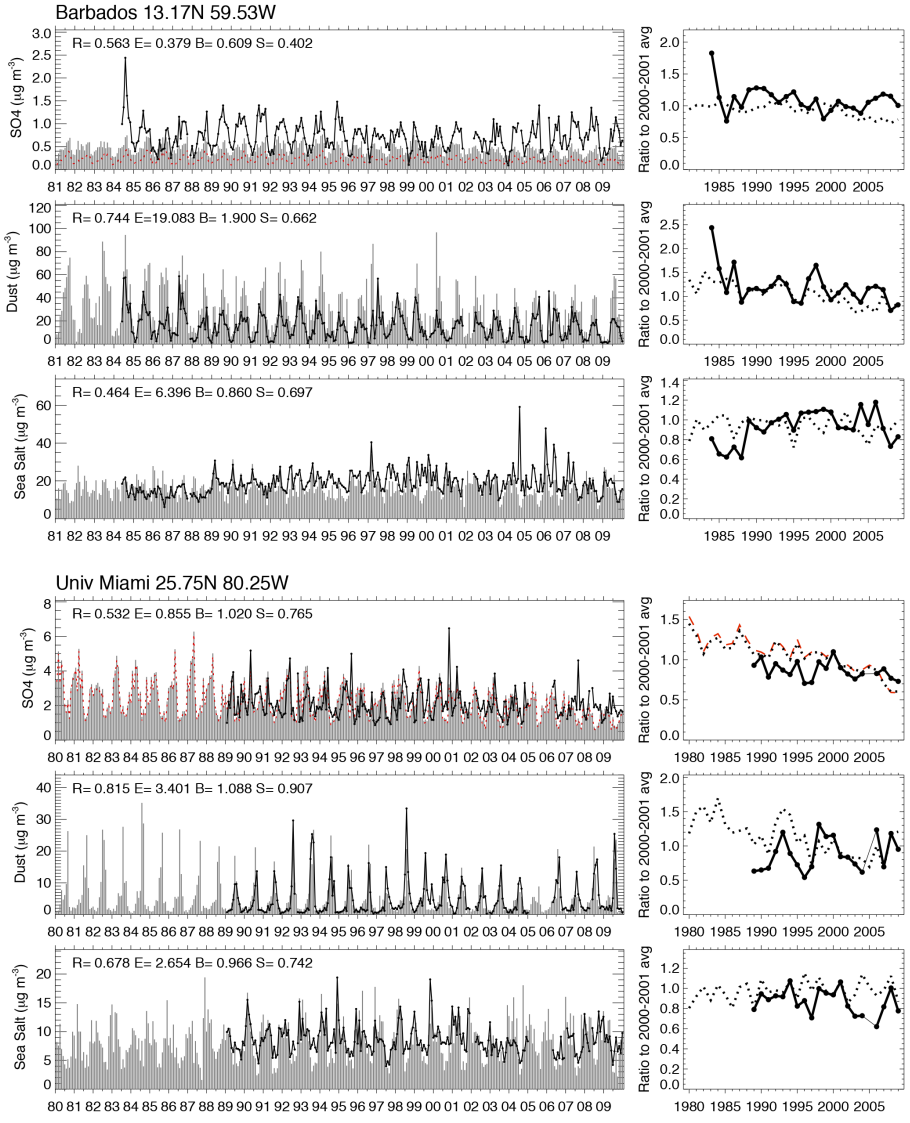

Fig. 10a. Left column: monthly averaged surface concentrations ($\mu g\,m^{-3}$) of non-sea-salt sulfate, dust, and sea salt from 1980 to 2009 at Barbados in North Atlantic (top three rows) and Miami on the coast of Florida (bottom three rows). Data from the University of Miami network. Observations are shown in black lines and the model results in grey bars for total amount and dotted red lines for FF+BB amount. Statistical measures (R, E, B, and S) are defined as the same as in Fig. 8a caption. Right column: corresponding ratio of annual mean concentrations to the 2000–2001 average showing the interannual variability/trend over the 20-year period with the observation and models in solid and dotted lines, respectively. Thin solid black line in the right column connects the points with missing year(s) in between for visual continuity.

Asia and southern Africa, a strong decrease over northern Africa and Brazil, and the hint of a decrease over Russia and Europe from its rather limited spatial coverage at high latitudes. Over North America, TOMS indicates an increase in the western US, with "hot spots" on the north and south borders possibly because of the difference in biomass burning between 2000–2001 and 1988–1989, and some decreasing tendency in the eastern US and southern Mexico.

In comparison, the total AOD change from GOCART during the first time segment (Fig. 11a, top right) is generally smaller (ΔAOD within ± 0.02) than that from satellite data over the ocean. Qualitatively, GOCART is consistent with the data, showing a decrease over the North Atlantic in mid- to high latitudes ($> 30°$ N) and subtropical areas off the west coast of northern Africa, and increases along the coast of central Africa, the northern Indian Ocean, and the western North Pacific. Over land, the model shows the largest AOD decreases over Europe, high latitudes of Eurasia and North America, and North Africa, whereas the largest increases occur over East and Central Asia as well as tropical/subtropical

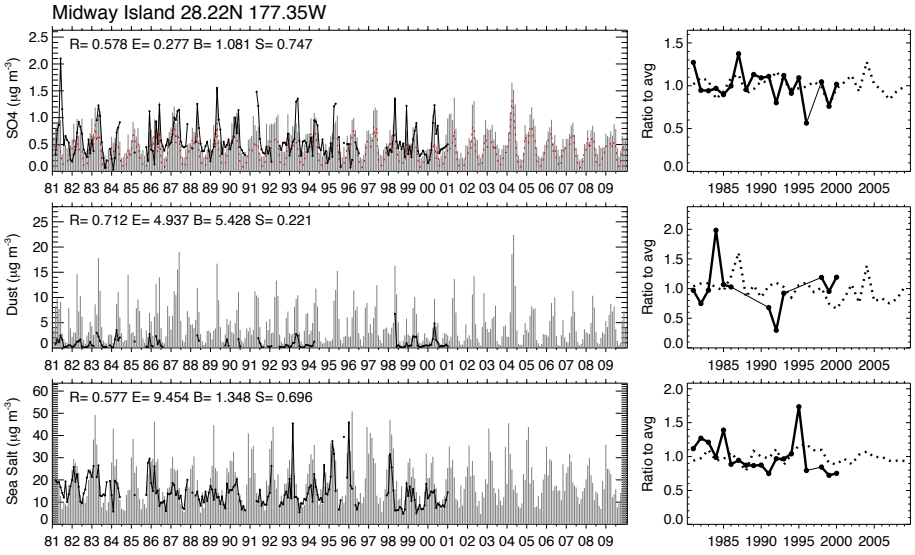

Fig. 10b. Same as Fig. 10a but for Midway Island in the North Pacific. Right column shows the ratio of annual mean concentrations to the average value over the available measurement years.

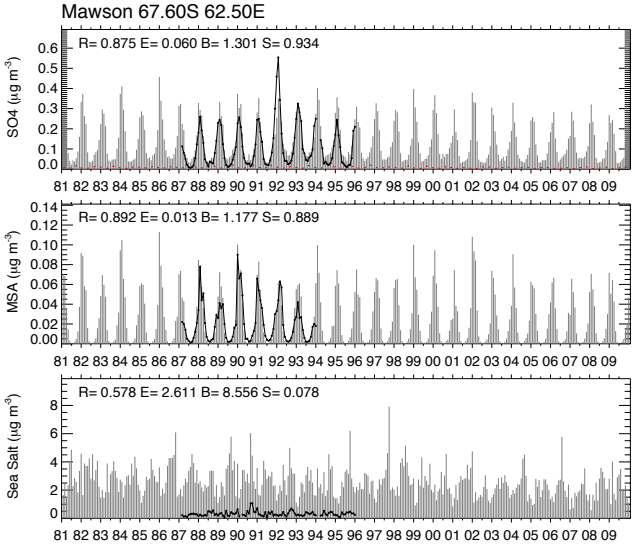

Fig. 10c. Same as Fig. 10b but for sulfate, MSA, and sea salt at Mawson Station on the Antarctic coast and without the ratio of annual mean to data average (data record is too short for deriving the trend).

Africa. The direction of these changes is generally consistent with the TOMS data with a few exceptions, although the magnitude is smaller. The model also displays a 0.05–0.1 AOD decrease over the Arctic, where no satellite data are available. From the simulation separating natural from FF+BB burning emissions (middle and lower panels in the right column of Fig. 11a), the model indicates that the changes over North America, Europe, Asia, and the Arctic are mainly due to combustion (mostly fossil fuel) emission changes, and, as we have seen in Fig. 6, the changes of dust and combustion AOD are in opposite directions over Central Asia and South Asia. The decrease over northern Africa and increase over central Asia reflect the change of dust whereas the increase in southern Japan is due to the volcanic activity from Miyakajima, which was quite active in 2000–2001 but not in 1988–1989 (http://www.volcano.si.edu/).

During the second time segment (Fig. 11b), the tendency of AOD change from AVHRR-CDR over the ocean is different from the first segment. In contrast with the decreasing AOD trends over large ocean areas during the first time segment, it shows an increasing trend in the range of 0.02–0.2 over the tropics and Southern Ocean near Antarctica, and a 0.02–0.05 decrease in the North Atlantic near the coastal regions. This pattern is different from other satellite products. All satellite data show an AOD increase over the northern Indian Ocean, with larger increases from AVHRR-CDR and MODIS-Terra (0.05–0.20) than from SeaWiFS and MISR (0.02–0.10). Over land, the three EOS satellite sensors all show an AOD decrease over the eastern US, Europe, South America, and southern Africa but an increase over eastern China and India. Over major dust regions (North Africa, the Middle East, and Central Asia), SeaWiFS and MISR in general show an increase, especially the "hot spot" of 0.1–0.2 AOD increase over the Arabian Peninsula from SeaWiFS, which occurred mostly in spring and summer (Hsu et al., 2012). Note that there are no MODIS-Terra Deep Blue products available for 2008 and 2009 over the deserts in Collection 5 used here.

The model, on the other hand, indicates a smaller AOD change (within ± 0.02) than satellite products over most oceanic areas in the second time segment, but shows a decrease off the west coast of northern and southern Africa that

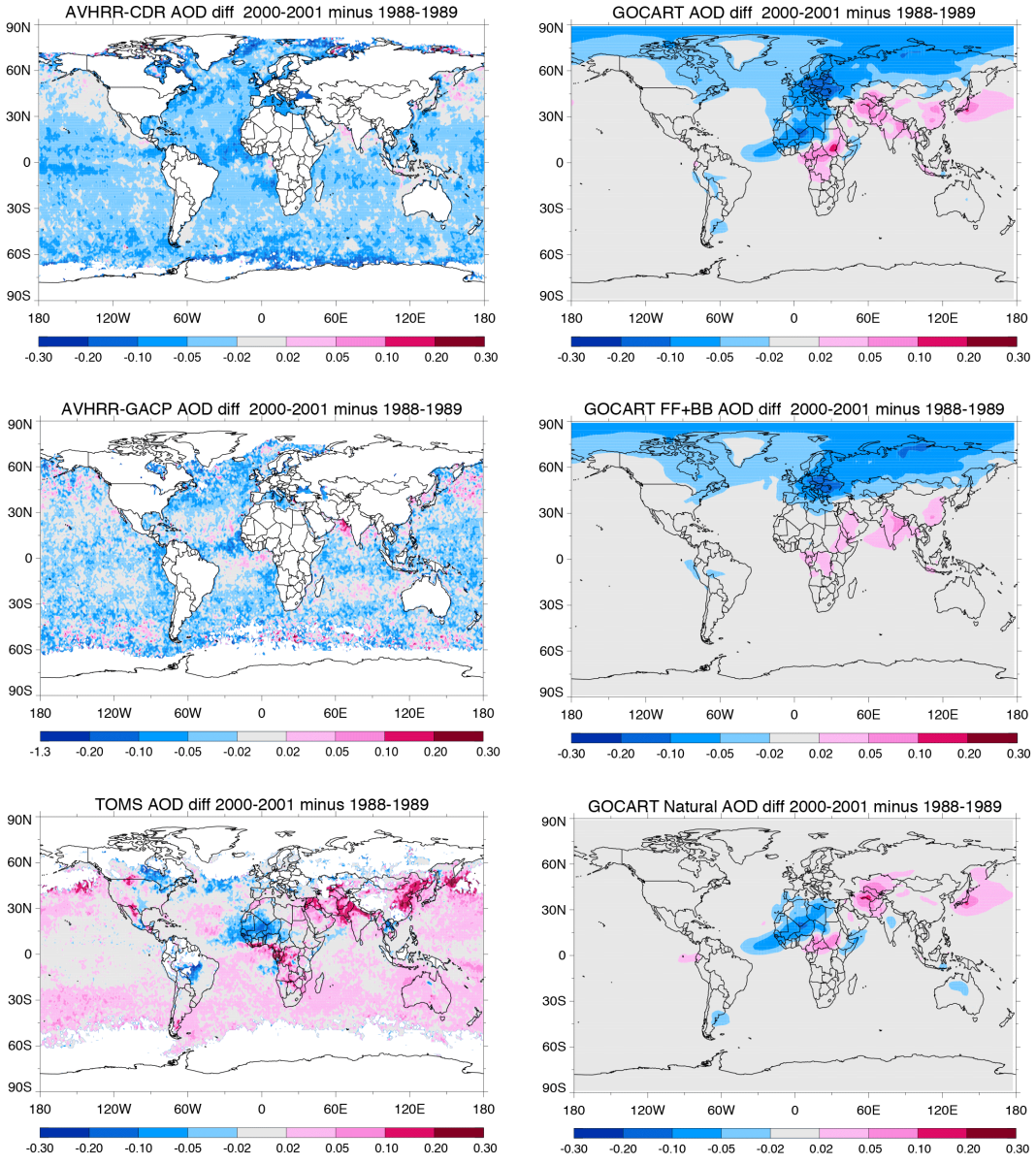

Fig. 11a. Difference of AOD between 2000–2001 and 1988–1989 from satellite data (left column, from top: AVHRR-CDR, AVHRR-GACP, and TOMS) and GOCART simulations (right column, from top: total, FF+BB, and natural AOD). White area indicates no data.

is similar to SeaWiFS and MISR, a decrease over the east coast of North America and west of central America that is consistent with AVHRR-CDR and MISR, and decreases in the northwest Pacific east of Japan, the Arctic Ocean, and the Southern Ocean near Antarctica that are either not evident from the satellite data or not observable by the satellites, possibly due to persistent cloud cover. Over land, the model shows a continuous decrease of AOD over the US, Europe and Russia and a continuous increase over East Asia and part of South Asia from the previous decade (Fig. 11a). Over the desert regions, the model also simulates an increase over North Africa, the Middle East, and Central Asia, in the same direction as the changes seen in SeaWiFS and MISR, although the increase in the Arabian Peninsula (0–0.05) is much weaker than the magnitudes from SeaWiFS (0.1–0.2) and MISR (0.02–0.1). Another intriguing change is in the dust source and outflow regions of North Africa and the tropical North Atlantic: the model shows that the AOD over the tropical North Atlantic has been decreasing in both time segments, despite the AOD increase in the upwind North African dust source regions in the second time segment. The model-calculated change in the latter time segment is supported by the SeaWiFS data and, to some extent, by the MISR data as

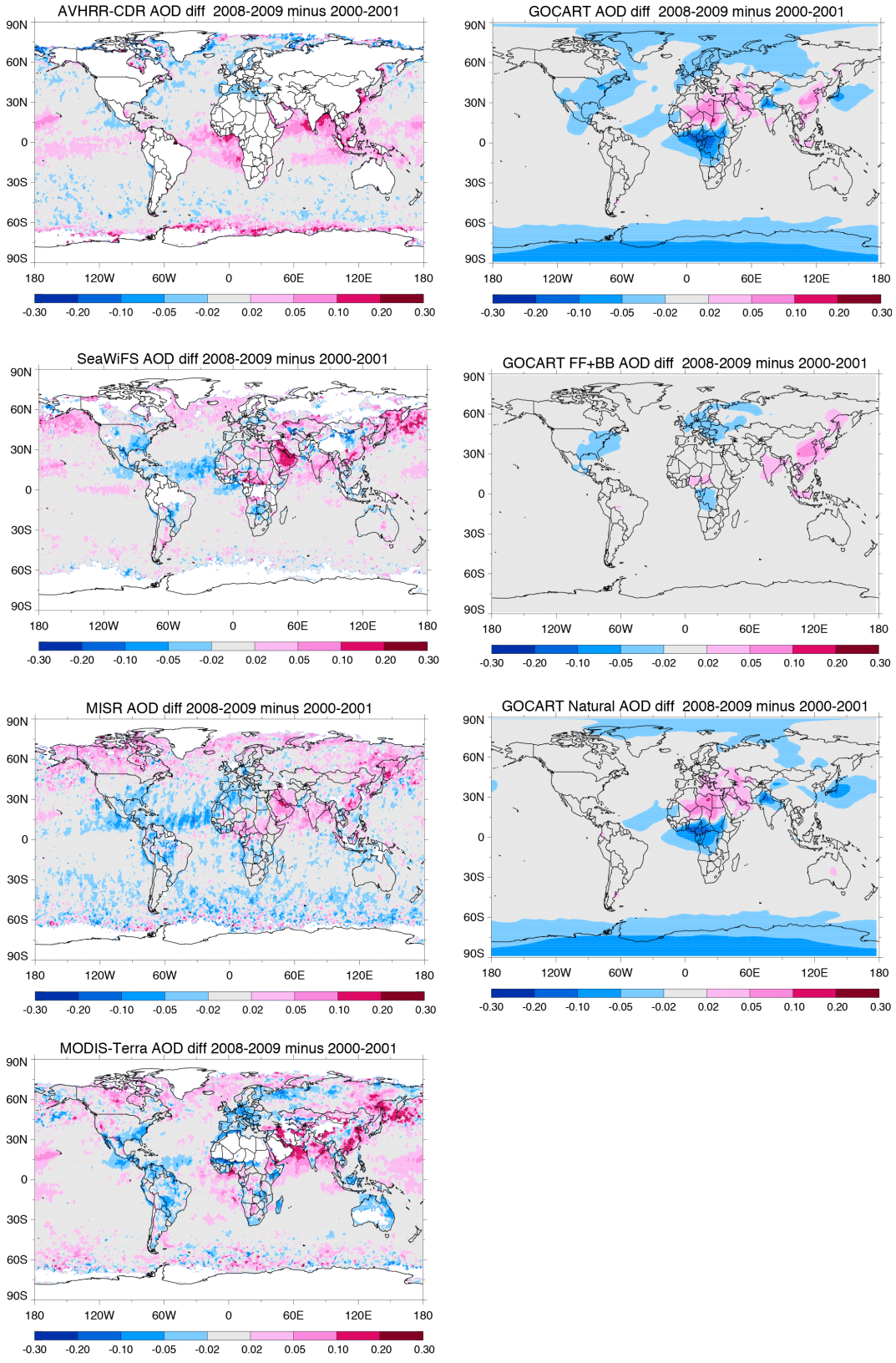

Fig. 11b. Difference of AOD between 2008–2009 and 2000–2001 from satellite data (left column, from top: AVHRR-CDR, SeaWiFS, MISR, and MODIS-Terra) and GOCART simulations (right column, from top: total, FF+BB, and natural AOD). White area indicates no data. The data gap over the desert regions in MODIS-Terra is due to the unavailability of Deep Blue products in 2008 and 2009.

well. We discuss the controlling factors of dust emission and transport in Sect. 5.2.

Although there are differences in the AOD changes in different satellite products, the data are usually consistent over land as well as the outflow regions over ocean, and can be explained mostly by the changes of land-based emissions. Satellite data have relatively larger uncertainties over remote areas because of low AOD, and additional difficulties at high latitudes due to the high reflective surfaces, low sun angle, and persistent cloud cover.

4.5 Synopsis of the results

Several key findings have emerged from the long-term data and model simulation shown in this section regarding trends:

- Over land, the most obvious 30-year trend is the reduction of aerosols in Europe. This reduction is primarily a decrease of anthropogenic aerosols resulting from the persistent efforts at pollution emission control that is also linked to a reduction in sulfate aerosol in both the eastern and western Arctic. Other significant AOD trends include an increase in combustion aerosol in the developing economies of Asia, which is partially offset by a dust component that either remains steady (EAS) or decreases (SAS). However, there is lack of long-term surface-based measurements available in EAS and SAS to further test the results. Fluctuations of AOD in dust and biomass burning regions occur during the 30-year record, with AOD increasing over CAS and MDE in the last 15 years but variable changes in Africa, and large year-to-year variations in biomass burning regions with no overall trends. Overlaid on all of this variability are the very strong changes imposed by large volcanic eruptions of El Chichón and Pinatubo.

- Over ocean, the AOD changes in the continental outflow areas in general appear to be in the same directions as their neighboring land, e.g., decrease over NAT and increase downwind of EAS. The most robust feature is the reduction of AOD in the dust outflow region of tropical North Atlantic, consistently shown in almost all satellite data and the model, a direction that may not be consistent with the AOD changes in North Africa. This weakening of dust transport from North Africa to the North Atlantic is also evident in the long-term surface dust concentration record at Barbados where the dust is predominantly from North Africa via the trans-Atlantic transport.

- Satellite products are mostly coherent over land regions with relatively dark surfaces. Over brighter surfaces where a significant amount of dust persists, the MODIS AOD products are generally 0.05–0.1 higher than SeaWiFS and MISR. Over ocean, AOD from MISR is always the highest, followed by MODIS-Terra, MODIS-Aqua, AVHRR, and SeaWiFS during their overlapping period. Although the differences in satellite AOD products are within their specified uncertainty or bias ranges, evaluation of models over areas with data discrepancies is difficult. Even so, we find the model falling outside the range of the different satellite data sets in the regions dominated by tropical biomass burning land regions and tropical oceans, where it underestimates AOD, and in dust-dominated regions, where it overestimates AOD.

5 Discussion

5.1 Relationships between emission, surface concentration, and AOD in polluted regions

To estimate the effects of changing emissions on AOD and surface concentration, it is necessary to examine the relationships between those quantities in different regions. Yet, such relationships can be influenced by many other factors other than regional emissions, such as transport (net import vs. net export), removal efficiency (dry vs. wet regions), source type (surface sources vs. higher-altitude sources), and source density (total emission per unit area). Thus, the relationship of emission-AOD-surface concentration can be quite different from region to region, and the regional AOD and/or surface concentrations may not be controlled by or respond linearly to regional emission changes. Nonetheless, to shed light on the plausible responses of atmospheric aerosol to emission changes on a regional basis, we simply show the relationships between emissions and model-calculated AOD or surface concentrations within four major anthropogenic source regions known to be net export regions: USA, EUR, EAS, and SAS. More quantitative assessments of local or regional aerosol source attributions and source-receptor relationships require additional model experiments that "tag" emissions based on source region and/or source type (e.g., Chin et al., 2007; HTAP 2010; Yu et al., 2013), an approach that is not covered here.

We select years that are not influenced by large volcanic eruptions (1980–1981, 1988–1990, 2002–2009) in order to concentrate on emissions predominantly within the PBL. We perform a linear fit between the total annual emissions and the annual averaged surface concentration or AOD within each region for sulfur (sulfate AOD, total sulfur emission), OM, and BC, as they are mostly generated from combustion sources. The correlation coefficient indicates how closely the concentrations or AOD reflect the regional emission, and the slope may suggest the change of concentration or AOD per unit change of regional emission. The results are shown in Fig. 12.

The emissions and surface concentrations in these regions exhibit a tight linear relationship on a regional and annual

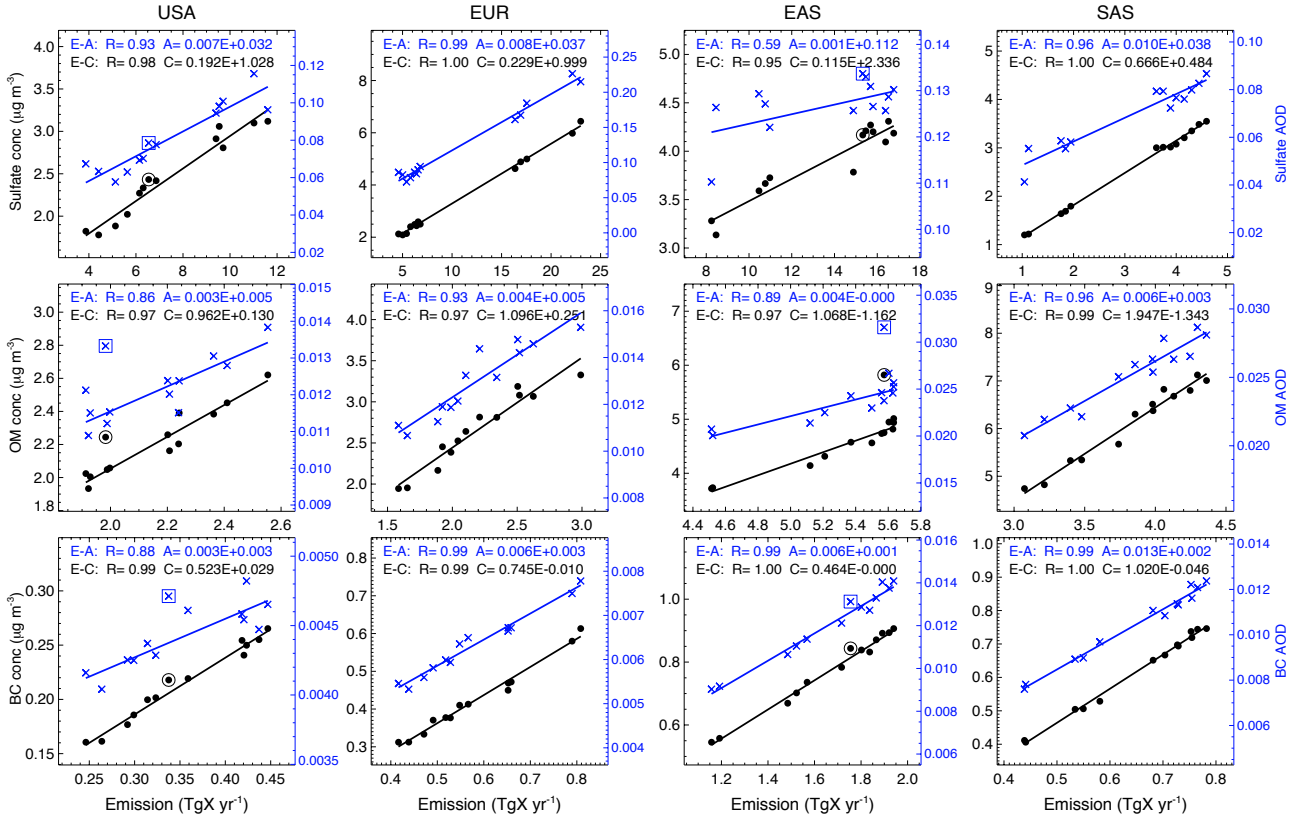

Fig. 12. Model-estimated relationship between emission (E) and surface concentrations (C) (black dots) or AOD (A) (blue crosses) of sulfur (total sulfur emissions, mainly SO_2, and sulfate concentration or AOD) (1st row), OM (2nd row), and BC (3rd row) on regional and annual average over USA (1st column), Europe (2nd column), East Asia (3rd column), and South Asia (4th column) in years without global-scale volcanic influence (1980–1981, 1988–1990, and 2002–2009). The year 2003 is excluded from the linear fitting in the USA and EAS (highlighted with large open circles for surface concentrations and open squares for AOD) because of the significant influence from the transport of the Russian wild fires (see text). Emissions are expressed as annual total within the individual regions in TgX year^{-1}, where X is S for sulfur and C for BC and OM.

average basis. Note the obvious outlier of OM concentration in East Asia (highlighted with the open circle) at nearly 6 μg m^{-3} in 2003, mostly due to OM imported from large boreal fires in eastern Russia during the spring and summer that year (Edwards et al., 2004; Generoso et al., 2007). The smoke plume from this fire not only strongly affects aerosol concentrations in East Asia, but also impacts that in the US (open circled) via trans-Pacific transport (e.g., Yu et al., 2008). Excluding results from 2003 makes emission and surface OM concentrations much better correlated in East Asia (R increased from 0.85 to 0.95) and the US (R increase from 0.93 to 0.97). The strong correlations (R well above 0.9) between emissions and surface concentrations for all species strongly imply that the air quality in those regions with respect to particulate pollution is mainly controlled by emissions within the region, as suggested by several previous studies (e.g., Chin et al., 2007; HTAP 2010).

In contrast, emissions and AOD are not as closely related, even though in Europe and South Asia the correlation coefficients are still high, in the range of 0.94 to 0.99. The looser correlations between regional emissions and AOD imply that long-range transport from extra-regional sources can be significant, as transported aerosol usually has a larger influence aloft than at the surface over receptor regions (e.g., Chin et al., 2007; Yu et al., 2012, 2013). For example, even with exclusion of the year 2003 (highlighted with open squares), the correlation coefficients between emissions and AOD for OM and BC over the US are 0.86 and 0.88, respectively, significantly lower than the 0.97 and 0.99 between emissions and surface concentrations. A previous modeling study estimated that BC from Asia could contribute up to 50 % of total BC at 2 km and an even higher percentage at higher elevation in spring (April 2004) off the west coast of North America (Hadley et al., 2007), although at higher altitudes BC concentrations are usually much lower than in the boundary layer. Another recent study found that intercontinental transport contributes about 28 % of BC AOD and 21 % of OM AOD over North America, averaged over 9 global models, that is dominated by the emissions from East Asia (Yu et al., 2013). Surprisingly, the weakest correlation between

emissions and AOD from the model is the sulfur over East Asia ($R = 0.59$ between SO_2 emission and sulfate AOD), a region that is known to be a major anthropogenic SO_2 source and net exporter of pollutants, especially in the recent decade, so a high correlation is expected. By examining the anthropogenic and natural components of sulfate AOD from regional and extra-regional sources, we find that natural volcanic aerosols play an important role in shifting the expected sulfur emission and sulfate AOD correlation in the model. There have been numerous active volcanoes in the Kamchatka Peninsula (Russian Territory, outside the EAS domain) that frequently release SO_2 into the atmosphere. These emissions can inject SO_2 to high altitudes to produce sulfate aerosol that can spread over a large area. For example, the 1981 Alaid volcano eruption was one of the largest on record in the Kuril Islands just south of Kamchatka, injecting about 1100 kilotons of SO_2 to near the tropopause. GOCART simulation shows sulfate aerosol from that eruption spreading to the Arctic and subarctic as well as the northern part of East Asia (Mongolia and northern China), and lasting for several months. On annual average for the years included in Fig. 12, extra-regional volcanic sources contribute 0.01–0.03 of sulfate AOD to the EAS region. If we only select sulfur from combustion sources, the correlation between SO_2 emission and sulfate AOD is much tighter ($R = 0.97$).

5.2 Factors controlling dust emission and loading

We examine two phenomena related to dust emission and transport: the plausible reasons for the changes of dust loading in North Africa, the Middle East, and Central Asia, and the continuous decrease of dust in the tropical North Atlantic (Fig. 11a and b). These changes seem to be consistent between multiple satellite observations and the model.

As we have described in Sect. 2, two key parameters that determine the dust emission are 10 m wind speed, $u_{10\,\mathrm{m}}$, and the ground wetness w – the stronger the $u_{10\,\mathrm{m}}$ and the lower the w, the larger the dust emission. Although $u_{10\,\mathrm{m}}$ is the driving force for lifting dust from the ground, w acts as a switch for dust emission depending on whether w is below (emission on) or above (emission off) a threshold value (currently 0.35 in GOCART). In addition, w also determines the dust uplifting threshold velocity u_t (Ginoux et al., 2001). We examine the dust emission and AOD changes calculated by GOCART and the meteorological variables $u_{10\,\mathrm{m}}$ and w from MERRA over major dust regions of North Africa (Sahara and Sahel), the Middle East, and Central Asia in Fig. 13. It indicates that w plays a more important role in regulating dust emission in Central Asia and the Middle East than in the Sahara and Sahel because the surface is generally wetter, especially in Central Asia, where dust emission seems to be mostly determined by the w region-wise (emission and w are negatively correlated with $R = -0.67$). Therefore, we attribute the increase of dust AOD in Central Asia in the last decade (2000–2009) mostly to a drier surface in the later years, whereas in the Middle East the change of dust emission responds to both u_{10m} and w changes, although the u_{10m} provides a stronger forcing. Figure 13 also shows a decreasing dust emission trend from the mid-1980s to the mid-2000s in both the Sahara (SHR) and Sahel (SHL), with a stronger decrease in the Sahel. This decrease can be attributed mostly to the weakening of the 10 m wind strength, considering the high correlation between the emission and 10 m winds over both regions. The model-calculated reduction of dust emissions and winds in the Sahel is supported by long-term observations (1984–2010) at seven World Meteorological Organization (WMO) weather stations in the Sahel, all showing decreasing 10 m wind speed (albeit to a larger degree than MERRA) and dust event frequency (Cowie et al., 2013).

The different AOD plots for selected time segments in Fig. 11 reveal that dust in the tropical North Atlantic decreased between the late 1980s and the late 2000s. This general decrease was reported in several previous studies that linked the decrease to an increase of sea surface temperature (SST) in the North Atlantic (Wong et al., 2008; Foltz and McPhaden, 2008; Wang et al., 2012) or the increased precipitation in the Sahel (Mishchenko and Geogdzhayev, 2007; Wang et al., 2012). Studies have also shown that dust export from North Africa is to some extent correlated with the North Atlantic Oscillation (NAO), a climate phenomenon in the North Atlantic Ocean that represents fluctuations in the sea level pressure difference between the Icelandic low and the Azores high (e.g., Hurrell, 1995; Hurrell et al., 2003); stronger dust outflow is expected with more positive NAO (e.g., Moulin et al., 1997; Ginoux et al., 2004; Chiapello et al., 2005). We examine in Fig. 14 (panel a to f) the correlations between the tropical North Atlantic dust AOD anomaly with the anomalies of dust emissions calculated by GOCART, precipitation and SST from MERRA, and the Hurrell annual NAO index. The regional scale correlations in Fig. 14 suggest that the dust AOD in the tropical North Atlantic is most positively correlated with the Sahel dust emission ($R = 0.72$) and mostly negatively correlated with the North Atlantic SST ($R = -0.69$); it is also correlated with dust emission in the Sahara ($R = 0.52$) and anti-correlated with precipitation (implying dust removal) over the tropical North Atlantic ($R = -0.58$). Although the dust AOD change seems to be associated with the phase and strength of the NAO, the correlation is not strong ($R = 0.44$). Therefore, the decreasing trend of dust AOD in the tropical North Atlantic during the past 30 years is probably driven by the large-scale climate forcing represented by the SST increase, which changes the surface pressure, atmospheric circulation, and precipitation, affecting dust emissions in the source region and transport to the North Atlantic. Although studies have pointed out that a warmer North Atlantic would produce wetter conditions and lower dust emission in Sahel, and thus less dust in the North Atlantic (Foltz and McPhaden, 2008; Wang et al., 2012), the MERRA reanalysis does not show increased precipitation over the Sahel (panel c in Fig. 14) as SST increases; rather,

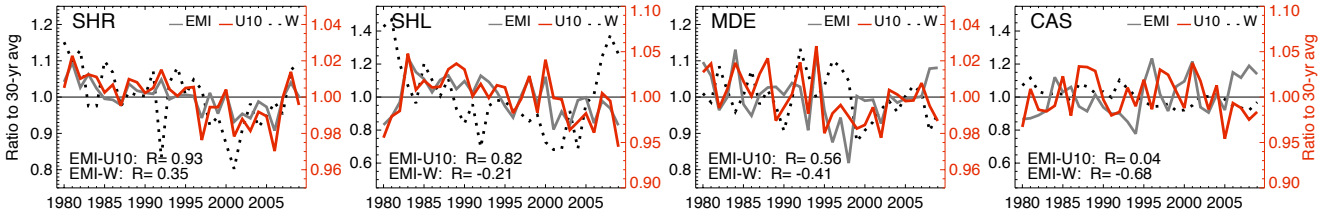

Fig. 13. Regional changes of GOCART dust emission (EMI, dark grey line) and its controlling parameters of 10 m wind speed (U10, red line) and ground wetness (W, dotted dark grey line) from MERRA from 1980 to 2009, expressed as ratios of annual averaged values to 30-year average, in four dust source regions of Middle East (top left), Central Asia (top right), Sahara (bottom left) and Sahel (bottom right). See Fig. 1 for region domains. Note the linear correlation coefficients on regional and annual average scale serve as indicators on the relative closeness between the emission and meteorological parameters.

it yields a positive precipitation trend over the North Atlantic that removes dust more efficiently. Our results show that the dust emission in the Sahel is more controlled by wind speeds than ground wetness (the latter is directly related to precipitation).

The model also suggests that change of North African dust emission and transport is directly responsible for the surface dust concentrations trends at Barbados and Miami, which are also tightly linked to the SST change. We show in the last two panels of Fig. 14 the relationship between the North Atlantic SST anomaly and the surface dust concentration anomaly at Barbados (panel g) and Miami (panel h) calculated by GOCART. We have also found that essentially there is no direct connection between the Sahel precipitation anomaly and the Barbados dust concentration anomaly in the 30-year time span ($R = 0.12$, not shown in Fig. 14), different from a previous study that suggested a close tie between the Sahel rainfall index and the Barbados dust concentration (Prospero and Lamb, 2003), although the correlations fall apart with the latest 25 years of data (Prospero and Mayol-Bracero, 2013). However, the MERRA precipitation trends might be influenced by a change over time of the observing system used in generating the reanalysis, rather than the "real" trends, especially over the ocean (Bosilovich et al., 2011). As such, our interpretation of the causal effects of dust trends may have to be reassessed after any inconsistencies induced by the observing system change in MERRA are removed (M. Bosilovich, personal communication, 2012).

5.3 Global and regional trends and attributions of combustion aerosols

Figure 15 plots the model-calculated average AOD and that from combustion sources in 15 land and 12 ocean regions (domains in Fig. 1) as well as the averages of global land, ocean, and the entire globe for four time slices of 1980, 1990, 2000, and 2009. It is to symbolize the global and regional changes of aerosols during the 30-year period. Among the major Northern Hemisphere pollution regions, Europe shows the largest reduction in combustion AOD fraction (−27 %) from 1980 to 2009, and South Asia shows the largest increase (+22 %). Over ocean, the largest reduction of combustion AOD fraction (−16 %) is over the northern part of the North Atlantic, whereas the largest increase takes place over the North Indian Ocean (+15 %), mostly resulting from emission changes over Europe and South Asia, respectively. Averaged over the global land area, the combustion source accounts for 38 % of AOD in 1980 and 33 % in 2009, whereas over ocean the corresponding percentages are 31 % and 27 %, respectively. The global average of about 30 % FF+BB fraction in this study is lower than our previous model simulation, which estimated the fraction at more than 40 % (Chin et al., 2009), largely because a much higher biomass burning emission (about 70 % higher) was used in that study. As we have seen in Figs. 6 and 7, our simulations suggest that the biomass burning emission from A2-ACCMIP in the present study may be too low.

Remarkably, despite large changes in emissions, the global averaged annual AOD values over land, ocean, and the entire globe only vary within ±0.01 in the years of decadal increments, which is in contrast with regional-scale changes in the source regions over land and continental downwind regions over ocean. This is because opposite trends over different regions cancel each other out in the global average, and there is little change over large open ocean areas. In addition, aerosol distribution is highly inhomogeneous; even on the annual, regional averaged scale the difference can be as large as a factor of 5 between the regions with the highest and lowest aerosol loading. Clearly, using global average values is not sufficient and not even useful for assessing aerosol trends and climate effects; such assessments should be performed at regional scales in a global context.

Results in Fig. 15 and our analysis in previous sections also suggest that there are trends and interannual variability of natural aerosols, such as dust and volcanoes. Anthropogenic aerosol forcing is considered as a perturbation of the natural state or "background." However, the background is not constant; it exhibits large spatial and temporal variations, creating challenges for anthropogenic forcing estimation, especially with measurement-based approaches that require detecting perturbation signals as deviations from the

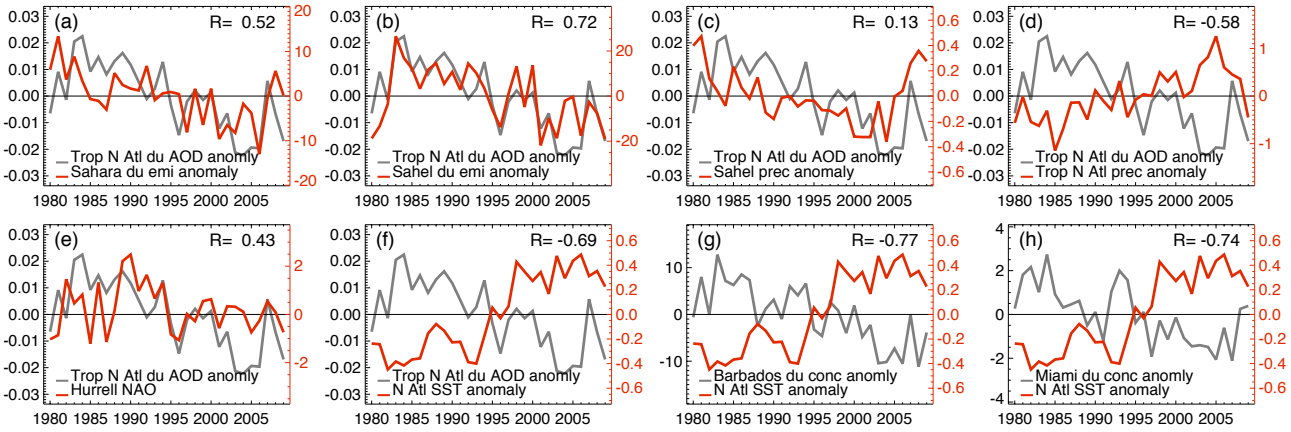

Fig. 14. From **(a)** to **(e)**: time series of GOCART-calculated tropical North Atlantic (5–20° N, 90–18° W) dust AOD anomaly (dark grey line) vs. (red line) model-calculated Sahara dust emission anomaly **(a)**, model-calculated Sahel dust emission anomaly **(b)**, MERRA Sahel precipitation anomaly **(c)**, MERRA tropical North Atlantic precipitation anomaly **(d)**, Hurrell principle component-based NAO index (http://climatedataguide.ucar.edu/guidance/hurrell-north-atlantic-oscillation-nao-index-pc-based) **(e)**, and MERRA North Atlantic (0–66° N) SST anomaly **(f)**. From **(g)** to **(h)**: time series of GOCART-calculated Barbados **(g)** and Miami **(h)** dust concentration anomaly vs. North Atlantic SST anomaly. Anomaly is defined as the difference between the annual average value and the 30-year mean.

natural background, and cannot directly distinguish aerosols from different origins.

6 Conclusions

We have presented an assessment of atmospheric aerosol sources and regional trends during the last three decades (1980–2009), based on the GOCART model analysis of multi-decadal, multi-platform data. Our analysis is performed over and downwind of major aerosol source regions or remote ocean regions, with land region domains determined mostly by geopolitical boundaries to better connect emission changes with the economic development and environmental policies within the geopolitical regions. The model results of AOD and surface concentration trends or variations have been compared with multiple satellite and ground-based measurements. During the past three decades, large volcanic eruptions of El Chichón in 1982 and Pinatubo in 1991 exerted profound and lasting effects on AOD everywhere on the globe, although they have had little impact on surface aerosol concentrations in places where they are measured. Our analysis concentrates on the years having minimal influence from Pinatubo or El Chichón.

Over land regions dominated by pollution aerosols, the 30-year AOD and surface concentration trends are generally consistent with the direction of the regional pollutant emission changes. All observations and the GOCART model show that the largest reductions of AOD and surface concentration have occurred over Europe, with the late 2000s AOD nearly half and surface sulfate concentration less than half of their values in the early 1980s. The US has also exhibited detectable AOD and surface concentration reductions. On the other hand, East Asia and South Asia show AOD increases. Even though these changes are in line with the combustion emission trends within the region, relatively large contributions of natural aerosols (dust, volcanic) in Asia make the total AOD changes less directly connected to pollutant emissions trends compared with Europe. Over the Arctic, the model and long-term surface measurements show a significant decrease of sulfate concentrations since the early 1990s, aligned with the decreasing trends over Europe, as the transport of European pollution was the main source of Arctic surface sulfate. Although long-range transport affects aerosol loading in regions downwind, the model shows that within polluted regions of the US, Europe, East Asia, and South Asia the surface concentrations of sulfate, BC, and OM aerosols are highly correlated with regional emissions, with correlation coefficients above 0.9. The correlation between regional emissions and AOD for a given species is less well correlated because of extra-regional aerosol contributions from long-range transport, especially for carbonaceous aerosols (BC and OM) over the US, presumably due to trans-Pacific transport from Asia, and sulfate over East Asia, seemingly from volcanic sources within and outside the region that usually remain aloft longer than boundary layer aerosols.

Over major dust source regions, model analysis of dust emission and its controlling parameters indicates that the change of dust emissions in the Sahara and Sahel responds mostly to near-surface wind speed changes, but in Central Asia, ground wetness is the primary influence. In the Middle East, both wind and ground wetness play important roles in regulating dust emissions. Although there is significant seasonal and interannual variability of dust distribution, both satellite observations and model simulations show a general

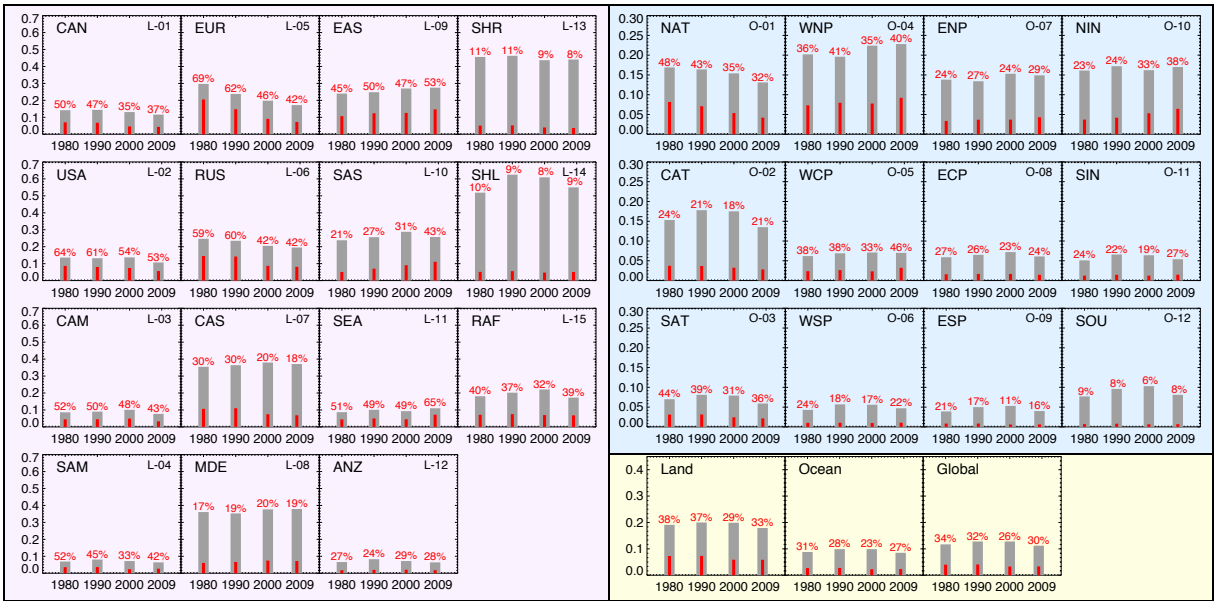

Fig. 15. Model-calculated average AOD (thick grey vertical bars) in decadal time slices, 1980, 1990, 2000, and 2009, over 15 land regions (pink panels, labeled "L-xx" where xx = 01–15), 12 ocean regions (light blue panels, labeled "O-xx" where xx = 01–12), and land, ocean, and global averages (light yellow panels). Region names listed in Table 1. Thin red vertical bars inside of the grey bars indicating the AOD from combustion (fossil fuel, biofuel, and biomass burning, or FF+BB) sources, with the number of percentage AOD from FF+BB shown in red color above each corresponding AOD bar.

decreasing trend of dust in the tropical Atlantic during the last three decades, which seems to be most closely related to a reduction of dust emission in North Africa, especially in the Sahel, and an increase of precipitation over the North Atlantic, both likely the result of a North Atlantic Ocean warming trend (SST increase) that drives atmospheric circulation and precipitation changes. The warming North Atlantic sea surface is found to be strongly connected to the decrease of not only the dust AOD in the tropical North Atlantic, but also the reduction of dust surface concentrations across the North Atlantic at Barbados and Miami.

Over most ocean areas other than the tropical North Atlantic, aerosol changes are generally much weaker than that over land, although close to the continents they are usually in the same direction as the adjacent land. The AOD changes among different satellite data over remote ocean can be inconsistent, primarily due to the low AOD values within the range of retrieval uncertainty.

Globally, the model estimates that aerosols from fossil fuel/biofuel combustion and biomass burning, collectively combustion aerosols that are mostly of anthropogenic origin, contribute about one-third to the mid-visible AOD, with a higher fraction over land than ocean, and higher in the 1980s than the 2000s. This fraction is likely to represent a lower limit, as the model generally underestimates biomass burning aerosols, excludes some anthropogenic aerosols such as nitrate and the secondary organic aerosol from anthropogenic sources, and overestimates dust aerosols.

Despite the significant changes in aerosol sources, concentrations, and AOD over many regions, model-calculated global averaged AOD values show little trends or variations over land and ocean on a global, annual scale, because increases and decreases in different land regions tend to cancel each other in the global average and little changes occur over large open ocean areas. A globally averaged number conceals not only opposing regional changes but also the large spatial inhomogeneity of aerosols. This highlights the need for regional-scale analyses, as global average values are not sufficient for assessing aerosol trends and impacts.

Our results also suggest that natural aerosols, such as dust and volcanic aerosol, play important roles in determining the regional and global aerosol changes even over major pollution source regions. The large spatial and temporal variations of the natural aerosol background impose a challenge to estimating the magnitude of anthropogenic perturbation and quantitatively determining the anthropogenic aerosol forcing, especially for measurement-based approaches that have difficulty distinguishing aerosols originating from anthropogenic or natural sources.

Supplementary material related to this article is available online at http://www.atmos-chem-phys.net/14/3657/2014/acp-14-3657-2014-supplement.pdf.

Acknowledgements. We thank the IMPROVE, EMEP, and AERONET networks for making their data available on line. Site PIs and data managers of these networks are gratefully acknowledged. We also thank the Goddard Earth Science Data and Information Services Center for providing gridded satellite products of SeaWiFS, MISR, and MODIS through their Giovanni website. We are grateful to three anonymous reviewers for their very constructive, helpful comments. This work is supported by NASA's Modeling, Analysis, and Prediction (MAP) program and the Atmospheric Composition, Modeling, and Analysis Program (ACMAP). X. Pan is supported by the NASA Postdoctoral Program, administrated by the Oak Ridge Associated University (ORAU).

Edited by: O. Dubovik

References

Bluth, G. J. S., Doiron, S. D., Schnetzler, C. C., Krueger, A. J., and Walter, L. S.: Global tracking of the sulfur dioxide clouds from the June, 1991 Mount Pinatubo eruptions, Geophys. Res. Lett., 19, 151–154, 1992.

Bosilovich, M. G., Robertson, F. R., and Chen, J.: Global energy and water budgets in MERRA, J. Climate, 24, 5721–5739, 2011.

Brown, M. E., Pinzon, J. E., Didan, K., Morisette, J. T., and Tucker, C. J.: Evaluation of the consistency of long-term NDVI time series derived from AVHRR, SPOT-Vegetation, SeaWIFS, MODIS and LandSAT ETM+, IEEE T. Geosci. Remote, 44, 1787–1793, 2006.

Chan, P. K., Zhao, X., and Heidinger, A. K.: Long-term aerosol climate data record derived from operational AVHRR satellite observations, Dataset Papers in Geosciences, 2013, 140791, doi:10.7167/2013/140791, 2013.

Chiacchio, M., Ewen, T., Wild, M., M. Chin, and Diehl, T.: Decadal variability of aerosol optical depth in Europe and its relationship to the temporal shift of the North Atlantic Oscillation in the realm of dimming and brightening, J. Geophys. Res., 116, D02108, doi:10.1029/2010JD014471, 2011.

Chiapello, I., Moulin, C., and Prospero, J. M.: Understanding the long-term variability of African dust transport across the Atlantic as recorded in both Barbados surface concentrations and large-scale Total Ozone Mapping Spectrometer (TOMS) optical thickness, J. Geophys. Res., 110, D18S10, doi:10.1029/2004JD005132, 2005.

Chin, M., Jacob, D. J., Gardner, G. M., Foreman-Fowler, M. S., Spiro, P. A., and Savoie, D. L.: A global three-dimensional model of tropospheric sulfate, J. Geophys. Res., 101, 18667–18690, 1996.

Chin, M., Rood, R. B., Lin, S.-J., Müller, J.-F., and Thompson, A. M.: Atmospheric sulfur cycle in the global model GOCART: Model description and global properties, J. Geophys. Res., 105, 24661–24687, 2000.

Chin, M., Ginoux, P., Kinne, S., Torres, O., Holben, B. N., Duncan, B. N., Martin, R. V.,Logan, J. A., Higurashi, A., and Nakajima, T.: Tropospheric aerosol optical thickness from the GOCART model and comparisons with satellite and sunphotometer measurements, J. Atmos. Sci., 59, 461–483, 2002.

Chin, M., Diehl, T., Ginoux, P., and Malm, W.: Intercontinental transport of pollution and dust aerosols: implications for regional air quality, Atmos. Chem. Phys., 7, 5501–5517, doi:10.5194/acp-7-5501-2007, 2007.

Chin, M., Diehl, T., Dubovik, O., Eck, T. F., Holben, B. N., Sinyuk, A., and Streets, D. G.: Light absorption by pollution, dust, and biomass burning aerosols: a global model study and evaluation with AERONET measurements, Ann. Geophys., 27, 3439–3464, doi:10.5194/angeo-27-3439-2009, 2009.

Collaud Coen, M., Andrews, E., Asmi, A., Baltensperger, U., Bukowiecki, N., Day, D., Fiebig, M., Fjaeraa, A. M., Flentje, H., Hyvärinen, A., Jefferson, A., Jennings, S. G., Kouvarakis, G., Lihavainen, H., Lund Myhre, C., Malm, W. C., Mihapopoulos, N., Molenar, J. V., O'Dowd, C., Ogren, J. A., Schichtel, B. A., Sheridan, P., Virkkula, A., Weingartner, E., Weller, R., and Laj, P.: Aerosol decadal trends – Part 1: In-situ optical measurements at GAW and IMPROVE stations, Atmos. Chem. Phys., 13, 869–894, doi:10.5194/acp-13-869-2013, 2013.

Cowie, S., Knippertz, P., and Marsham, J.: Are vegetation-related roughness changes the cause of the recent decrease in dust emission from Sahel?, Geophys. Res. Lett., 40, 1868–1872, doi:10.1002/grl.50273, 2013.

Dey, S. and Di Girolamo, A.: A decade of change in aerosol properties over the Indian subcontinent, Geophys. Res. Lett., 38, L14811, dio:10.1029/2011GL048153, 2011.

Diehl, T., Heil, A., Chin, M., Pan, X., Streets, D., Schultz, M., and Kinne, S.: Anthropogenic, biomass burning, and volcanic emissions of black carbon, organic carbon, and SO_2 from 1980 to 2010 for hindcast model experiments, Atmos. Chem. Phys. Discuss., 12, 24895–24954, doi:10.5194/acpd-12-24895-2012, 2012.

Dubovik, O., Sinyuk, A., Lapyonok, T., Holben, B. N., Mishchenko, M., Yang, P., Eck, T. F., Volten, H., Muñoz, O., Veihelmann, B., van der Zande, W. J., Leon, J.-F., Sorokin, M., and Slutsker, I.: Application of spheroid models to account for aerosol particle nonsphericity in remote sensing of desert dust, J. Geophys. Res., 111, D11208, doi:10.1029/2005JD006619, 2006.

Eck, T. F., Holben, B. N., Reid, J. S., Dubovik, O., Smirnov, A., O'Neill, N. T., Slutsker, I., and Kinne, S.: Wavelength dependence of the optical depth of biomass burning, urban, and desert dust aerosols, J. Geophys. Res., 104, 31333–31349, 1999.

Edwards, D. P., Emmons, L. K., Hauglustaine, D. A., Chu, D. A., Gille, J. C., Kaufman, Y. J., Pétron, G., Yurganov, L. N., Giglio, L., Deeter, M. N., Yudin, V., Ziskin, D. C., Warner, J., Lamarque, J.-F., Francis, G. L., Ho, S. P., Mao, D., Chen, J., Grechko, E. I., and Drummond, J. R.: Observations of carbon monoxide and aerosols from the Terra satellite: Northern Hemisphere variability, J. Geophys. Res., 109, D24202, doi:10.1029/2004JD004727, 2004.

Foltz, G. R. and McPhaden, M. J.: Trends in Saharan dust and tropical Atlantic climate during 1980–2006, Geophys. Res. Lett., 35, L20706, doi:10.1029/2008GL035042, 2008.

Gantt, B., Meskhidze, N., Facchini, M. C., Rinaldi, M., Ceburnis, D., and O'Dowd, C. D.: Wind speed dependent size-resolved parameterization for the organic mass fraction of sea spray aerosol, Atmos. Chem. Phys., 11, 8777–8790, doi:10.5194/acp-11-8777-2011, 2011.

Generoso, S., Bey, I., Attie, J.-L., and Bréon, F.-M.: A satellite- and model-based assessment of the 2003 Russian fires: Impact on the Arctic region, J. Geophys. Res., 112, D15301, doi:10.1029/2006JD008344, 2007.

Ginoux, P., Chin, M., Tegen, I., Prospero, J., Holben, B., Dubovik, O., and Lin, S.-J.: Sources and global distributions of dust aerosols simulated with the GOCART model, J. Geophys. Res., 106, 20255–20273, 2001.

Ginoux, P., Prospero, J., Torres, O., and Chin, M.: Long-term simulation of dust distribution with the GOCART model: Correlation with the North Atlantic Oscillation, Environ. Modell. Softw., 19, 113–128, 2004.

Gong, S.: A parameterization of sea-salt aerosol source function for sub- and super-micron particles, Global Biogeochem. Cy., 17, 1097, doi:10.1029/2003GB002079, 2003.

Granier, C., Bessagnet, B., Bond, T., D'Angiola, A., van der Gon, H. D., Frost, G. J., Heil, A., Kaiser, J. W., Stefan Kinne, S., Klimont, Z., Kloster, S., Lamarque, J.-F., Liousse, C., Masui, T., Meleux, F., Mieville, A., Ohara, T., Raut, J.-C., Riahi, K., Schultz, M. G., Smith, S. J., Thompson, A., van Aardenne, J., van der Werf , G. R., and van Vuuren, D. P.: Evolution of anthropogenic and biomass burning emissions of air pollutants at global and regional scales during the 1980–2010 period, Climatic Change, 109, 163–190, doi:10.1007/s10584-011-0154-1, 2011.

Guenther, A., Hewitt, C. N., Erickson, D., Fall, R., Geron, C., Graedel, T., Harley, P., Klinger, L., Lerdau, M., Mckay, W. A., Pierce, T., Scholes, B., Steinbrecher, R., Tallamraju, R., Taylor, J., and Zimmerman, P. A.: Global-Model of Natu- ral Volatile Organic-Compound Emissions, J. Geophys. Res., 100, 8873–8892, 1995.

Hadley, O. L., Ramanathan, V., Carmichael, G. R., Tang, Y., Corrigan, C. E., Roberts, G. C., and Mauger, G. S.: Trans-Pacific transport of black carbon and fine aerosols ($D < 2.5\,\mu$m) into North America, J. Geophys. Res., 112, D05309, doi:10.1029/2006JD007632, 2007.

Herman, J. R., Bhartia, P. K., Torres, O., Hsu, C., and Seftor, C.: Global distribution of UV-absorbing aerosols from Nimbus 7/TOMS data, J. Geophys. Res., 102, 16911–16922, 1997.

Holben, B. N., Eck, T. F., Slutsker, I., Tanre, D., Buis, J. P., Setzer, A., Vermote, E., Reagan, J. A., Kaufman, Y., Nakajima, T., Lavenu, F., Jankowiak, I., and Smirnov, A.: AERONET – A federated instrument network and data archive for aerosol characterization, Remote Sens. Environ., 66, 1–16, 1998.

Holben, B. N., Tanre, D., Smirnov, A., Eck, T. F., Slutsker, I., Abuhassan, N., Newcomb, J., Schafer, W. W., Chatenet, B., Lavenue, F., Kaufman, Y. J., Vande Castle, J., Setzer, A., Markham, B., Clark, D., Frouin, R., Halthore, R., Karnieli, A., O'Neill, N. T., Pietras, C., Pinker, R. T., Voss, K., and Zibordi, G.: An emerging ground-based aerosol climatology: Aerosol optical depth from AERONET, J. Geophys. Res., 106, 12067–12097, 2001.

Hsu, N. C., Herman, J. R., Bhartia, P. K., Seftor, C. J., Torres, O., Thompson, A. M., Gleason, J. F., Eck, T. F., and Holben, B. N.: detection of biomass burning smoke from TOMS measurements, Geophys. Res. Lett., 23, 745–748, 1996.

Hsu, N. C., Tsay, S.-C., King, M. D., and Herman, J. R.: Aerosol properties over bright-reflecting source regions, IEEE T. Geosci. Remote, 42, 557–569, 2004.

Hsu, N. C., Gautam, R., Sayer, A. M., Bettenhausen, C., Li, C., Jeong, M. J., Tsay, S.-C., and Holben, B. N.: Global and regional trends of aerosol optical depth over land and ocean using SeaWiFS measurements from 1997 to 2010, Atmos. Chem. Phys., 12, 8037–8053, doi:10.5194/acp-12-8037-2012, 2012.

HTAP 2010: Hemispheric Transport of Air Pollution 2010. Part A: Ozone and Particulate Matter, Air Pollution Studies No. 17, edited by: Dentener, F., Keating, T., and Akimoto, H., United Nations, New York, 2010.

Hurrell, J. W.: Decadal trend in the North Atlantic Oscillation: Regional temperatures and precipitations, Science, 269, 676–679, 1995.

Hurrell, J. W., Kushnir, Y., Visbeck, M., and Ottersen, G.: An overview of the North Atlantic Oscillation, in: The North Atlantic Oscillation, Climatic Significance and Environmental Impact, edited by: Hurrell, J. W., Kushnir, Y., Ottersen, G., and Visbeck, M., AGU Geophysical Monograph, vol. 134, 1–35, 2003.

Husar, R. B., Prospero, J. M., and Stowe, L. L.: Characterization of tropospheric aerosols over the oceans with the NOAA advanced very high resolution radiometer optical thickness operational prod- uct, J. Geophys. Res., 102, 16889–16909, 1997.

Jaeglé, L., Quinn, P. K., Bates, T. S., Alexander, B., and Lin, J.-T.: Global distribution of sea salt aerosols: new constraints from in situ and remote sensing observations, Atmos. Chem. Phys., 11, 3137–3157, doi:10.5194/acp-11-3137-2011, 2011.

Kahn, R. A., Garay, M. J., Nelson, D. L., Yau, K. K., Bull, M. A., Gaitley, B. J.,Martonchik, J. V., and Levy, R. C.: Satellite-derived aerosol optical depth over dark water from MISR and MODIS: Comparisons with AERONET and implications for climatological studies, J. Geophys. Res., 112, D18205, doi:10.1029/2006JD008175, 2007.

Kahn, R. A., Nelson, D. L., Garay, M., Levy, R. C., Bull, M. A., Diner, D. J., Martonchik, J. V., Paradise, S. R., Hansen, E. G., and Remer, L. A.: MISR Aerosol product attributes, and statistical comparisons with MODIS, IEEE T. Geosci. Remote, 47, 4095–4114, 2009.

Kahn, R. A., Gaitley, B. J., Garay, M. J., Diner, D. J., Eck, T., Smirnov, A., and Holben, B. N.: Multiangle Imaging SpectroRadiometer global aerosol product assessment by comparison with the Aerosol Robotic Network, J. Geophys. Res., 115, D23209, doi:10.1029/2010JD014601, 2010.

Kalashnikova, O. V., Garay, M. J., Martonchik, J. V., and Diner, D. J.: MISR Dark Water aerosol retrievals: operational algorithm sensitivity to particle non-sphericity, Atmos. Meas. Tech., 6, 2131–2154, doi:10.5194/amt-6-2131-2013, 2013.

Karnieli, A., Derimian, Y., Indoitu, R., Panov, N., Levy, R. C., Remer, L. A., Maenhaut, W., and Holben, B. N.: Temporal trend in anthropogenic sulfur aerosol transport from central and eastern Europe to Israel, J. Geophys. Res., 114, D00D19, doi:10.1029/2009JD011870, 2009.

Kaufman, Y. J., Tanré, D., Remer, L., Vermote, E., Chu, A., and Holben, B. N.: Operational remote sensing of tropospheric aerosol over land from EOS moderate resolution imaging spectroradiometer, J. Geophys. Res., 102, 17051–17067, 1997.

Kaufman, Y. J., Boucher, O., Tanré, D., Chin, M., Remer, L. A., and Takemura, T.: Aerosol anthropogenic component estimated from satellite data, Geophys. Res. Lett., 32, L17804, doi:10.1029/2005GL023125, 2005.

Kim, D., Chin, M., Bian, H., Tan, Q., Brown, M. E., Zheng, T., You, R., Diehl, T., Ginoux, P., and Kucsera, T.: The effect of the dynamic surface bareness on dust source function, emission, and distribution, J. Geophys. Res., 118, 1–16, doi:10.1029/2012JD017907, 2013.

Koch, D., Jacob, D., Tegen, I., Rind, D., and Chin, M.: Tropospheric sulfur simulations and sulfate direct radiative forcing in the GISS GCM, J. Geophys. Res., 104, 23799–23823, 1999.

Lamarque, J.-F., Bond, T. C., Eyring, V., Granier, C., Heil, A., Klimont, Z., Lee, D., Liousse, C., Mieville, A., Owen, B., Schultz, M. G., Shindell, D., Smith, S. J., Stehfest, E., Van Aardenne, J., Cooper, O. R., Kainuma, M., Mahowald, N., McConnell, J. R., Naik, V., Riahi, K., and van Vuuren, D. P.: Historical (1850–2000) gridded anthropogenic and biomass burning emissions of reactive gases and aerosols: methodology and application, Atmos. Chem. Phys., 10, 7017–7039, doi:10.5194/acp-10-7017-2010, 2010.

Lana, A., Bell, T. G., Simó, R., Vallina, S. M., Ballabrera-Poy, J., Kettle, A. J., Dachs, J., Bopp, L., Saltzman, E. S., Stefels, J., Johnson, J. E., and Liss, P. S.: An updated climatology of surface dimethlysulfide concentrations and emission fluxes in the global ocean, Global Biogeochem. Cy., 25, GB1004, doi:10.1029/2010GB003850, 2011.

Leibensperger, E. M., Mickley, L. J., Jacob, D. J., Chen, W.-T., Seinfeld, J. H., Nenes, A., Adams, P. J., Streets, D. G., Kumar, N., and Rind, D.: Climatic effects of 1950–2050 changes in US anthropogenic aerosols – Part 1: Aerosol trends and radiative forcing, Atmos. Chem. Phys., 12, 3333–3348, doi:10.5194/acp-12-3333-2012, 2012.

Levy, R. C., Remer, L. A., Kleidman, R. G., Mattoo, S., Ichoku, C., Kahn, R., and Eck, T. F.: Global evaluation of the Collection 5 MODIS dark-target aerosol products over land, Atmos. Chem. Phys., 10, 10399–10420, doi:10.5194/acp-10-10399-2010, 2010.

Levy, R. C., Mattoo, S., Munchak, L. A., Remer, L. A., Sayer, A. M., Patadia, F., and Hsu, N. C.: The Collection 6 MODIS aerosol products over land and ocean, Atmos. Meas. Tech., 6, 2989–3034, doi:10.5194/amt-6-2989-2013, 2013.

Luo, Y., Lu, D., Zhou, X., Li, W., and He, Q.: Characteristics of the spatial distribution and yearly variation of aerosol optical depth over China in last 30 years, J. Geophys. Res., 106, 14501–14513, 2001.

Malm, W. C., Sisler, J. F., Huffman, D., Eldred, R. A., and Cahill, T. A.: Spatial and seasonal trends in particle concentration and optical extinction in the United States, J. Geophys. Res., 99, 1347–1370, 1994.

Malm, W. C., Day, D. E., Kreidenweis, S. M., Collett, J. L., and Lee, T.: Humidity-dependent optical properties of fine particles during the Big Bend Regional Aerosol Visibility Observational Study, J. Geophys. Res., 108, 4279, doi:10.1029/2002JD002998, 2003.

Maring, H., Savoie, D., Izaguirre, M., McCormick, C., Arimoto, R., Prospero, J., and Pilinis, C.: Aerosol Physical and Optical Properties and their Relationship to Aerosol Composition in the Free Troposphere at Izaña, Tenerife, Canary Islands during July 1995, J. Geophys. Res., 105, 14677–14700, 2000.

Massie, S. T., Torres, O., and Smith, S. J.: Total Ozone Mapping Spectrometer (TOMS) observations of increases in Asian aerosol in winter from 1979 to 2000, J. Geophys. Res., 109, D18211, doi:10.1029/2004JD004620, 2004.

McClain, C. R., Cleave, M. L., Feldman, G. C., Gregg, W. W., Hooker, S. B., and Kuring, N.: Science quality SeaWiFS data for global biospheric research, Sea Technol., 39, 10–16, 1998.

McCormick, M., Thomason, L. W., and Trepte, C. R.: Atmospheric effects of the Mt Pinatubo eruption, Nature, 373, 399–404, 1995.

Mishchenko, M. I. and Geogdzhayev, I. V.: Satellite remote sensing reveals regional tropospheric aerosol trends, Opt. Express, 15, 7423–7438, 2007.

Mishchenko, M. I., Travis, L. D., Kahn, R. A., and West, R. A.: Modeling phase functions for dustlike tropospheric aerosols using a shape mixture of randomly oriented polydisperse spheroids, J. Geophys. Res., 102, 16831–16847, doi:10.1029/96JD02110, 1997.

Mishchenko, M. I., Geogdzhayev, I. V., Cairns, B., Rossow, W. B., and Lacis, A. A.: Aerosol retrievals over the ocean using channel 1 and 2 AVHRR data: A sensitivity analysis and preliminary results, Appl. Opt., 38, 7325–7341, doi:10.1364/AO.38.007325, 1999.

Mishchenko, M. I., Geogdzhayev, I. V., Rossow, W. B., Cairns, B., Carlson, B. E.,Lacis, A. A., Liu, L., and Travis, L. D.: Long-term satellite record reveals likely recent aerosol trend, Science, 315, 1543, doi:10.1126/science.1136709, 2007.

Mishchenko, M. I., Liu, L., Geogdzhayev, I. V., Li, J., Carlson, B. E., Lacis, A. A., Cairns, B., and Travis, L. D.: Aerosol retrievals from channel-1 and -2 AVHRR radiances: Long-term trends updated and revisited, J. Quant. Spectrosc. Ra., 113, 1974–1980, 2012.

Moorthy, K. K., Babu, S. S., Manoj, M. R., and Satheesh, S. K.: Buildup of aerosols over the Indian Region, Geophys. Res. Lett, 40, 1011–1014, doi:10.1002/grl.50165, 2012.

Moulin, C., Lambert, C. E., Dulac, F., and Dayan, U.: Control of atmospheric export of dust from North Africa by the North Atlantic Oscillation, Nature, 387, 691–694, 1997.

Murphy, D. M., Chow, J. C., Leibensperger, E. M., Malm, W. C., Pitchford, M., Schichtel, B. A., Watson, J. G., and White, W. H.: Decreases in elemental carbon and fine particle mass in the United States, Atmos. Chem. Phys., 11, 4679–4686, doi:10.5194/acp-11-4679-2011, 2011.

Nakajima, T. and Higurashi, A.: A use of two-channel radiances for an aerosol characterization from space, Geophys. Res. Lett., 25, 3815–3818, 1998.

Petrenko, M., Kahn, R., Chin, M., Soja, A., Kucsera, T., and Harshvardhan: The use of satellite-measured aerosol optical depth to constrain biomass burning emissions source strength in a global model GOCART, J. Geophys. Res., 117, D18212, doi:10.1029/2012JD017870, 2012.

Prospero, J. M.: Long-range transport of mineral dust in the global atmosphere: Impact of African dust on the environment of the southeastern United States, P. Natl. Acad. Sci. USA, 96, 3396–3403, 1999.

Prospero, J. M. and Lamb, P. J.: African droughts and dust transport to the Caribbean: Climate change implications, Science, 302, 1024–1027, 2003.

Prospero, J. M. and Mayol-Bracero, O. L.: Understanding the transport and impact of African dust on the Caribbean basin, B. Am. Meteorol. Soc., 94, 1329–1337, 2013.

Prospero, J. M., Savoie, D. L., Saltzman, E. S., and Larsen, R.: Impact of oceanic sources of biogenic sulphur on sulphate aerosol concentrations at Mawson, Antarctica, Nature, 350, 221–223, 1991.

Prospero, J. M., Savoie, D. L., and Arimoto, R.: Long-term record of nss-sulfate and nitrate in aerosols on Midway Island, 1981–2000: evidence of increased (now decreasing?) an-

thropogenic emissions from Asia, J. Geophys. Res., 108, 4019, doi:10.1029/2001JD001524, 2003.

Quinn, P. K., Shaw, G., Andrews, E., Dutton, E. G., Ruoho-Airola, T., and Gong, S. L.: Arctic haze: current trends and knowledge gaps, Tellus, 59, 99–114, 2007.

Quinn, P. K., Bates, T. S., Baum, E., Doubleday, N., Fiore, A. M., Flanner, M., Fridlind, A., Garrett, T. J., Koch, D., Menon, S., Shindell, D., Stohl, A., and Warren, S. G.: Short-lived pollutants in the Arctic: their climate impact and possible mitigation strategies, Atmos. Chem. Phys., 8, 1723–1735, doi:10.5194/acp-8-1723-2008, 2008.

Rahn, K. A.: Relative importance of North America and Eurasia as sources of Arctic aerosol, Atmos. Environ., 15, 1447–1455, 1981.

Ramachandran, S., Kedia, S., and Srivastava, R.: Aerosol optical depth trends over different regions of India, Atmos. Environ., 49, 338–347, 2012.

Remer, L. A., Kaufman, Y. J., Tanré, D., Mattoo, S., Chu, D. A., Martins, J. V., Li, R.-R., Ichoku, C., Levy, R. C., Kleidman, R. G., Eck, T. F., Vermote, E., and Holben, B. N.: The MODIS aerosol algorithm, products, and validation, J. Atmos. Sci., 62, 947–973, 2005.

Remer, L. A., Kleidman, R. G., Levy, R. C., Kaufman, Y. J., Tanré, D., Mattoo, S., Martins, J. V., Ichoku, C., Koren, I., Yu, H., and Holben, B. N.: Global aerosol climatology from the MODIS satellite sensors, J. Geophys. Res.-Atmos., 113, D14S07, doi:10.1029/2007JD009661, 2008.

Riahi, K., Rao, S., Krey, V., Cho, C., Chirkov, V., Fischer, G., Kindermann, G., Nakicenovic, N., and Rafaj, P.: RCP 8.5 – A scenario of comparatively high greenhouse gas emissions, Climatic Change, 109, 33–57, doi:10.1007/s10584-011-0149-y, 2011.

Rienecker, M. M., Suarez, M. J., Gelaro, R., Todling, R., Bacmeister, J., Liu, E., Bosilovich, M. G., Schubert, S. D., Takacs, L., Kim, G.-K., Bloom, S., Chen, J., Collins, D., Conaty, A., da Silva, A., Gu, W., Joiner, J., Koster, R. D., Lucchesi, R., Molod, A., Owens, T., Pawson, S., Pegion, P., Redder, C. R., Reichle, R., Robertson, F. R., Ruddick, A. G., Sienkiewicz, M., and Woollen, J.: MERRA – NASA's Modern-Era Retrospective Analysis for Research and Applications, J. Climate, 24, 3624–3648, 2011.

Savoie, D. L., Prospero, J. M., Larsen, R. J., and Saltzman, E. S.: Nitrogen and sulfur species in aerosols at Mawson, Antarctica, and their relationship to natural radionuclides, J. Atmos. Chem., 14, 181–204, 1992.

Savoie, D. L., Arimoto, R., Keene, W. C., Prospero, J. M., Duce, R. A., and Galloway, J. N.: Marine biogenic and anthropogenic contributions to nonseasalt sulfate in the marine boundary layer over the North Atlantic Ocean, J. Geophys. Res., 107, 4356, doi:10.1029/2001JD000970, 2002.

Sayer, A. M., Hsu, N. C., Bettenhausen, C., Ahmad, Z., Holben, B. N., Smirnov, A., Thomas, G. E., and Zhang, J.: SeaWiFS Ocean Aerosol Retrieval (SOAR): Algorithm, validation, and comparison with other data sets, J. Geophys. Res., 117, D03206, doi:10.1029/2011JD016599, 2012.

Shaw, G. E. and Stamnes: K.: Arctic haze: perturbation of the Polar radiation budget, Am. NY. Acad. Sci., 338, 533–539, 1980.

Shindell, D. T., Chin, M., Dentener, F., Doherty, R. M., Faluvegi, G., Fiore, A. M., Hess, P., Koch, D. M., MacKenzie, I. A., Sanderson, M. G., Schultz, M. G., Schulz, M., Stevenson, D. S., Teich, H., Textor, C., Wild, O., Bergmann, D. J., Bey, I., Bian, H., Cuvelier, C., Duncan, B. N., Folberth, G., Horowitz, L. W., Jonson, J., Kaminski, J. W., Marmer, E., Park, R., Pringle, K. J., Schroeder, S., Szopa, S., Takemura, T., Zeng, G., Keating, T. J., and Zuber, A.: A multi-model assessment of pollution transport to the Arctic, Atmos. Chem. Phys., 8, 5353–5372, doi:10.5194/acp-8-5353-2008, 2008.

Sillmann, J., Pozzoli, L., Vignati, E., Kloster, S., and Feichter, J.: Aerosol effect on climate extremes in Europe under different future scenarios, Geophys. Res. Lett., 40, 2290–2295, doi:10.1002/grl.50459, 2013.

Smirnov, A., Holben, B. N., Giles, D. M., Slutsker, I., O'Neill, N. T., Eck, T. F., Macke, A., Croot, P., Courcoux, Y., Sakerin, S. M., Smyth, T. J., Zielinski, T., Zibordi, G., Goes, J. I., Harvey, M. J., Quinn, P. K., Nelson, N. B., Radionov, V. F., Duarte, C. M., Losno, R., Sciare, J., Voss, K. J., Kinne, S., Nalli, N. R., Joseph, E., Krishna Moorthy, K., Covert, D. S., Gulev, S. K., Milinevsky, G., Larouche, P., Belanger, S., Horne, E., Chin, M., Remer, L. A., Kahn, R. A., Reid, J. S., Schulz, M., Heald, C. L., Zhang, J., Lapina, K., Kleidman, R. G., Griesfeller, J., Gaitley, B. J., Tan, Q., and Diehl, T. L.: Maritime aerosol network as a component of AERONET – first results and comparison with global aerosol models and satellite retrievals, Atmos. Meas. Tech., 4, 583–597, doi:10.5194/amt-4-583-2011, 2011.

Stowe, L. L., Ignatov, A. M., and Singh, R. R.: Development, validation and potential enhancements to the second generation operational aerosol product at NOAA/NESDIS, J. Geophys. Res., 102, 16923–16934, 1997.

Streets, D. G., Wu, Y., and Chin, M.: Two-decadal aerosol trends as a likely explanation of the global dimming/brightening transition, Geophys. Res. Lett., 33, L15806, doi:10.1029/2006GL026471, 2006.

Tanré, D., Kaufman, Y. J., Herman, M., and Mattoo, S.: Remote sensing of aerosol properties over oceans using the MODIS/EOS spectral radiances, J. Geophys. Res., 102, 16971–16988, doi:10.1029/96JD03437, 1997.

Taylor, K. E.: Summarizing multiple aspects of model performance in a single diagram, J. Geophys. Res., 106, 7183–7192, 2001.

Thomas, G. E., Poulsen, C. A., Siddans, R., Sayer, A. M., Carboni, E., Marsh, S. H., Dean, S. M., Grainger, R. G., and Lawrence, B. N.: Validation of the GRAPE single view aerosol retrieval for ATSR-2 and insights into the long term global AOD trend over the ocean, Atmos. Chem. Phys., 10, 4849–4866, doi:10.5194/acp-10-4849-2010, 2010.

Torres, O., Herman, J. R., Ahmad, Z., and Gleason, J.: Derivation of aerosol properties from satellite measurements of back- scattered ultraviolet radiation: Theoretical basis, J. Geophys. Res., 103, 17099–17110, 1998.

Torres, O., Bhartia, P. K., Herman, J. R., Sinyuk, A., Ginoux, P., and Holben, B.: A long-term record of aerosol optical depth from TOMS observations and comparison to AERONET measurements, J. Atmos. Sci., 59, 398–413, 2002.

Torres, O., Bhartia, P. K., Sinyuk, A., Welton, E. J., and Holben, B.: Total Ozone Mapping Spectrometer measurements of aerosol absorption from space: Comparison to SAFARI 2000 ground-based observations, J. Geophys. Res., 110, D10S18, doi:10.1029/2004JD004611, 2005.

Toth, T. D., Zhang, J., Campbell, J. R., Reid, J. S., Shi, Y., Johnson, R. S., Smirnov, A., Vaughan, M. A., and Winker, D. M.: Investigating enhanced Aqua MODIS aerosol optical depth retrievals

over the mid-to-high latitude Southern Oceans through intercomparison with co-located CALIOP, MAN, and AERONET data sets, J. Geophys. Res., 118, 4700–4714, doi:10.1002/jgrd.50311, 2013.

Tucker, C. Pinzon, J., J. E., Brown, M. E., Slayback, D., Pak, E. W., Mahoney, R., Vermote, E., and El Saleous, N.: An extended AVHRR 8-km NDVI data set compatible with MODIS and SPOT vegetation NDVI data, Int. J. Remote Sens., 26, 4485–4498, 2005.

Wang, C., Dong, S., Evan, A. T., Foltz, G. R., and Lee, S.-K.: Multidecadal covariability of North Atlantic sea surface temperature, African dust, Sahel rainfall, and Atlantic hurricanes, J. Climate, 25, 5404–5415, 2012.

Wong, S., Dessler, A. E., Mahowald, N. M., Colarco, P. R., and da Silva, A.: Long-term variability in Saharan dust transport and its link to North Atlantic sea surface temperature, Geophys. Res. Lett., 35, L07812, doi:10.1029/2007GL032297, 2008.

Yu, H., Remer, L. A., Chin, M., Bian, H., Kleidman, R. G., and Diehl, T.: A satellite-based assessment of transpacific transport of pollution aerosol, J. Geophys. Res., 113, D14S12, doi:10.1029/2007JD009349, 2008.

Yu, H., Chin, M., Remer, L.A., Kleidman, R. G., Bellouin, N., Bian, H., and Diehl, T.: Variability of marine aerosol fine-mode fraction and estimates of anthropogenic aerosol component over cloud-free oceans from the Moderate resolution Imaging Spectroradiometer (MODIS), J. Geophys. Res., 114, D10206, doi:10.1029/2008JD010648, 2009.

Yu, H., Remer, L., Chin, M., Bian, H., Tan, Q., Yuan, T., and Zhang, Y.: Aerosols from Overseas Rival Domestic Emissions over North America, Science, 337, 566–569, 2012.

Yu, H., Chin, M., West, J. J., Atherton, C. S., Bellouin, N., Bergmann, D., Bey, I., Bian, H., Diehl, T., Forberth, G., Hess, P., Schulz, M., Shindell, D., Takemura, T., and Tan, Q.: A multimodel assessment of the influence of regional anthropogenic emission reductions on aerosol direct radiative forcing and the role of intercontinental transport, J. Geophys. Res., 118, 700–720, doi:10.1029/2012JD018148, 2013.

Zhang, J. and Reid, J. S.: MODIS Aerosol product analysis for data assimilation: Assessment of Level 2 aerosol optical thickness retrievals, J. Geophys. Res, 111, D22207, doi:10.1029/2005JD006898, 2006.

Zhang, J. and Reid, J. S.: A decadal regional and global trend analysis of the aerosol optical depth using a data-assimilation grade over-water MODIS and Level 2 MISR aerosol products, Atmos. Chem. Phys., 10, 10949–10963, doi:10.5194/acp-10-10949-2010, 2010.

Zhao, X.-P., Laszlo, I., Guo, W., Heidinger, A., Cao, C., Jelenak, A., Tarpley, D., and Sullivan, J.: Study of long-term trend in aerosol optical thickness observed from operational AVHRR satellite instrument, J. Geophys. Res., 113, D07201, doi:10.1029/2007JD009061, 2008.

Zhao, X.-P., Chan, P. K., and Heidinger, A. K.: A global survey of the effect of cloud contamination on the aerosol optical thickness and its long-term trend derived from operational AVHRR satellite observations, J. Geophys. Res., 118, 2849–2857, doi:10.1002/jgrd.50278, 2013.